Anticyclonic eddies connecting the western boundaries of Indian and Atlantic oceans

R. Laxenaire[1], S. Speich[1], B. Blanke[2], A. Chaigneau[3,4,5], C. Pegliasco[3], and A. Stegner[1]

.

[1]Laboratoire de Météorologie Dynamique, UMR 8539 École Polytechnique, ENS, CNRS, Paris, France
[2]Laboratoire d,Océanographie Physique et Spatiale, UMR 6523, CNRS, Ifremer, IRD, UBO, Brest, France
[3]Laboratoire d,Etudes en Géophysique et Océanographie Spatiales, UMR CNES, CNRS, IRD, UPS, Toulouse, France
[4]Institut de Recherches Halieutiques et Océanologiques du Bénin (IRHOB), Cotonou, Bénin
[5]International Chair in Mathematical Physics and Applications (ICMPA-UNESCO Chair), University of Abomey-Calavi, Cotonou, Republic of Benin

Key Points:

- New eddy-tracking method including the detection of merging and splitting events improves estimates of eddies from satellite-mapped fields.
- Agulhas Rings show a very complex behavior with much longer lifespan and geographical range than previously observed.
- They play a major role in efficiently connecting western boundary currents of the South Indian and Atlantic oceans.

Corresponding author: Rémi Laxenaire, `rlaxe@lmd.ens.fr`

Abstract

(Added: The)Indo-Atlantic interocean exchanges achieved by Agulhas Rings (Deleted: ~~,~~) are tightly (Replaced: ~~related~~ replaced with: linked) to global ocean circulation and climate. Yet, they are still poorly understood(Replaced: ~~, as~~ replaced with: because) they are difficult to identify and follow. (Replaced: ~~Here we propose a new~~ replaced with: We propose here an original) assessment on Agulhas Rings, achieved by (Replaced: ~~a novel~~ replaced with: TOEddies, a new) eddy identification and tracking algorithm(Replaced: ~~, TOEddies,~~ replaced with: that we) applied (Replaced: ~~on~~ replaced with: over) 24 years of satellite altimetry. (Replaced: ~~The major novelty of the method~~ replaced with: Its main novelty) lies in the detection of eddy splitting and merging events. (Replaced: ~~The robustness of TOEddies is assessed by a systematic procedure that test the presence and properties of eddies against an independent eddy dataset derived from surface drifting buoys. Due to the many eddy-eddy interactions and the resulting eddy subdivisions and coalescences, the concept of a trajectory associated with a single eddy becomes meaningless. To be able to track the origins, fate and changes of Agulhas Rings we have defined a network of segments and trajectories that has enabled to reconstruct their routes and history. They reveal to be particularly complex and long, highlighting a higher turbulent nature than previously evaluated. We uncovers different origins and pathways for these eddies, their first positions being in the Indian Ocean upstream of the Agulhas Retroflection, and the farthest one in the most southwestern area of the Atlantic. Many of these eddies disappear from the altimetry signal in the Cape Basin. Yet, a significant fraction can be followed for years as they cross the entire South Atlantic and flow south with the Brazil Current.~~ replaced with: These are particularly abundant and significantly impact the concept of a trajectory associated with a single eddy, which becomes less obvious than previously admitted. To overcome this complication, we have defined a network of segments that group together in relatively complex trajectories. Such a network provides an original assessment of the routes and history of Agulhas Rings. It links 730 481 eddies into 6 363 segments that cluster into Agulhas Ring trajectories of different orders. Such an order depends on the affiliation of the eddies and segments, in a similar way as a tree of life. Among them, we have identified 122 “order 0” trajectories that can be considered as the major trajectories associated to a single eddy, albeit it has undergone itself splitting and merging events. Despite the disappearance of many eddies in the altimeter signal in the Cape Basin, a sig-

nificant fraction can be followed from the Indian Ocean to the South Brazil Current with, on average, 3.5 years to cross the entire South Atlantic.)

1 Introduction

Mesoscale eddies and meanders are ubiquitous structures in the ocean and are one of the major sources of ocean variability [*Stammer*, 1997; *Wunsch*, 1999]. They are thought to (Replaced: ~~be a major contributor~~ replaced with: contribute significantly) to the transfer of heat, salt, mass and biogeochemical properties across the World Ocean [*McWilliams*, 1985]. South of Africa, large mesoscale eddies [*Lutjeharms*, 2006], the so(Replaced: ~~-~~ replaced with:)called Agulhas Rings, are shed from the Agulhas Current into the Cape Basin at the Agulhas Retroflection [*Olson and Evans*, 1986; *Lutjeharms and Gordon*, 1987; *Lutjeharms and Ballegooyen*, 1988; *Gordon and Haxby*, 1990; *Rae*, 1991] transporting Indian waters into the Southeast Atlantic [*Ballegooyen et al.*, 1994; *Garzoli et al.*, 1999; *Arhan et al.*, 1999, 2011] affecting the heat, salt and biogeochemistry of the Atlantic Ocean [*Gordon et al.*, 1992; *Lehahn et al.*, 2011; *Paul et al.*, 2015; *Villar et al.*, 2015]. They participate in the Agulhas Leakage [*Ruijter et al.*, 1999; *Lutjeharms*, 2006], the Indo-Atlantic interocean exchange of water that (Replaced: ~~strongly impacts~~ replaced with: has a strong impact on) the Atlantic Meridional Overturning Circulation (AMOC), (Deleted: ~~by~~)influencing its strength [*Weijer et al.*, 1999, 2002; *van Sebille and van Leeuwen*, 2007], stability [*Weijer et al.*, 2001] and variability [*Biastoch et al.*, 2008a; *Biastoch and Böning*, 2013]. Therefore, the origins, number and fate of Agulhas Rings are key elements in assessing global ocean circulation and its variations in a changing climate.

Since 1992 several altimetry satellites have revealed the richness, complexity, and some surface properties of (Deleted: ~~the~~)mesoscale ocean dynamics [*Hernandez et al.*, 1995; *Chelton et al.*, 2007, 2011]. (Replaced: ~~From~~ replaced with: Based on) these data, a number of studies have estimated eddies and their trajectories(Added: ,) mainly from (Replaced: ~~medium~~ replaced with: mid) to high(Replaced: ~~-~~ replaced with:)latitude using various automatic eddy detection algorithms [e.g., *Isern-Fontanet et al.*, 2006; *Doglioli et al.*, 2007; *Chelton et al.*, 2007; *Chaigneau et al.*, 2008; *Nencioli et al.*, 2010; *Chelton et al.*, 2011; *Mason et al.*, 2014; *Faghmous et al.*, 2015; *Ashkezari et al.*, 2016; *Matsuoka et al.*, 2016; *Qiu-Yang et al.*, 2016; *Le Vu et al.*, 2018]. All these detection methods are based (Replaced: ~~on either~~ replaced with: either on) physical criteria (such as the estimation of the Okubo-Weiss parameter [*Okubo*, 1970; *Weiss*, 1991]) or geometrical properties of the flow (Deleted: ~~field~~). Several of these methods and eddy atlases are proposed to the scientific community and are made public (Deleted: ~~ally available~~). However, to (Deleted: ~~the best of~~)our knowledge, none of them (Replaced: ~~was~~ replaced with: were) quantitatively qualified against independent data. Efforts have been made to evaluate one or more methods, but this evaluation has been undertaken at a very local scale or using subjective assessments. *Souza et al.* [2011b], for example, have attempted to compare and validate three different detection methods using current knowledge of (Deleted: ~~eddies in the~~)South Atlantic (Replaced: ~~Ocean~~ replaced with: eddies) as independent criteria. *Chaigneau et al.* [2008] and *Faghmous et al.* [2015] compared their detection to structures identified by various experts. However, this procedure proved to be very sensitive, as (Deleted: ~~the~~)experts often disagreed. Finally, *Mkhinini et al.* [2014] and *Casanova-Masjoan et al.* [2017] undertook a more objective, albeit still qualitative, assessment of the skill of their (Replaced: ~~results~~ replaced with: method) by using respectively, 10 and 2 surface drifters trapped in specific anticyclonic eddies.

Using different eddy detection methods, several authors have attempted to reconstruct and analyze Agulhas Rings trajectories in and across the South Atlantic [e.g. *Gordon and Haxby*, 1990; *Byrne et al.*, 1995; *Souza et al.*, 2011a; *Wang et al.*, 2015]. In the published studies, most reconstructions of (Added: the trajectories of)Agulhas Rings (Deleted: ~~trajectories~~)leaving the Cape Basin are identified initially well (Replaced: ~~inside~~ replaced with: within) the Cape Basin and not at the Agulhas Current Retroflection where they are (Replaced: ~~supposed~~ replaced with: believed) to originate [e.g. *Byrne et al.*, 1995; *Souza et al.*, 2011a; *Wang et al.*, 2015, 2016; *Guerra et al.*, Submitted]. Taking into account the separation of an eddy into smaller structures, to which, in what follows, we will refer to as an eddy splitting event, *Dencausse et al.* [2010a] tracked (Added: the)Agulhas Rings formed in the Agulhas Retroflection area (Added: and)entering (Deleted: ~~in~~)the Cape Basin. They (Replaced: ~~showed~~ replaced with: have shown) that such events are very frequent. Indeed, the ratio obtained between the number of trajectories formed after a split and the number of trajectories tracked from the Agulhas Retroflection is close to 1. This process has an impact on the concept of Agulhas Ring trajectories and on the number of Agulhas Rings formed per year (traditionally estimated between 3 and 6) [e.g *Gordon and Haxby*, 1990; *Ballegooyen et al.*, 1994; *Byrne et al.*, 1995; *Goni et al.*, 1997]. In fact, *Dencausse et al.* [2010a] have shown that up to 14 Agulhas Rings per year enter the Cape Basin. However, these authors have only followed Agulhas Rings in a very limited region without addressing the question of (Replaced: ~~how~~ replaced with: the impact of) these eddy-eddy interactions (Deleted: ~~have an impact~~) on the recovery of the full extent of Agulhas Rings trajectories. For example, *Schouten et al.* [2002] showed that certain eddies formed in the Mozambique Channel or at the southern (Replaced: ~~edge~~ replaced with: limit) of Madagascar can, in addition to triggering Natal Pulses, be advected until the Retroflection (Added: region)leading to (Replaced: ~~a~~ replaced with: shedding of an) Agulhas Ring (Deleted: ~~-shedding~~). Downstream (Replaced: ~~of~~ replaced with: from) the Cape Basin, most of the Agulhas Rings described in the literature do not cross the South Atlantic entirely. To our knowledge, the only exceptions are a trajectory followed by *Byrne et al.* [1995] that reached 40°W near the American Margin and (Replaced: ~~one~~ replaced with: another) by *Guerra et al.* [Submitted] that clearly drifted south (Deleted: ~~ward~~) along the Brazilian coast (Deleted: ~~s~~). All these individual regional pictures of Agulhas Ring trajectories must, in (Replaced: ~~a~~ replaced with: one) way or another, be incorporated into a global vision taking into account (Deleted: ~~the~~)eddy-eddy interactions.

In this article, we present a new eddy(Replaced: ~~-~~ replaced with:)detection and tracking algorithm applied to the 24(Replaced: ~~–~~ replaced with: -)year satellite altimetry time series in a space domain covering the South Atlantic and Southwest Indian oceans. The eddy detection and tracking steps of this new algorithm (Replaced: ~~is a further~~ replaced with: are a) development of the geometric method of *Chaigneau et al.* [2008], *Chaigneau et al.* [2009], and *Pegliasco et al.* [2015]. To obtain an objective measure of the capabilities of our method and the robustness of our eddy database, we have developed a systematic procedure that tests the presence and properties of eddies against a totally independent data set, (Deleted: ~~the~~)so(Replaced: ~~-~~ replaced with:)called (Added: the)"loopers", which are (Deleted: ~~the~~)upper-ocean eddies identified from surface drifters and provided by *Lumpkin* [2016].

While the method is developed (Deleted: ~~for~~)and tested on all (Deleted: ~~the~~)eddies detected in the (Replaced: ~~study domain~~ replaced with: domain of study), particular emphasis will be placed on the results concerning the Agulhas Rings. Indeed, the new eddy detection and tracking method (Replaced: ~~provides~~ replaced with: gives) access to an unprecedented assessment of the origin (Deleted: ~~s~~) and fate of (Added: the)Agulhas Rings and the Indo-Atlantic exchange of waters they carry out. Moreover, we will discuss their characteristics and variations along the trajectories in terms of various kinematic and dynamical properties that can be deduced from altimetry.

The paper is organized as follows. In Section (Replaced: ~~2~~ replaced with: 2), the data we have used are described and the methods we have developed are presented. Validation and comparisons of our eddy(Replaced: ~~-~~ replaced with:)detection algorithm with a published databases are presented in Section (Replaced: ~~3. Section 4~~ replaced with: **??**. Section **??**) focuses on the Agulhas Rings. We discuss their origins, their disappearance from the altimetry field, their (Replaced: ~~pathways~~ replaced with: trajectories), and statistics on the different properties of Agulhas Rings. In the last section, the results are discussed and we draw the (Replaced: ~~major~~ replaced with: main) conclusions of this study.

2 Data and Methods

2.1 Satellite Altimetry Data

This study is based on more than 24 years (01/1993 to 05/2017) of daily (Added: maps of)delayed time absolute dynamic topography (ADT) (Deleted: ~~maps~~)and derived geostrophic velocity fields in the South Atlantic and Southeast Indian oceans [70°W-65°E; 55°S-15°S] (see Figure 1). These maps are produced by Ssalto/Duacs and distributed by the Copernicus Marine Environment Monitoring Service (http://marine.copernicus.eu/) in the version released in April 2014 (DT14) [*Duacs/AVISO+*, 2014; *Pujol et al.*, 2016]. They correspond to the gridded Sea Surface Height (SSH) above the geoid calculated by combining all (Added: the)data recorded by the (Deleted: ~~available~~)satellites (Added: available)among the 12 altimetric missions (Topex/Poseidon, ERS-1 and -2, Jason-1, OSTM/Jason-2, SARAL/Altika, Cryosat-2, Envisat, Geosat, Haiyang-2A, Jason-3 and Sentinel-3A). Objectively mapped ADT is the sum of Sea-Level Anomalies (SLA) and (Deleted: ~~the~~)Mean Dynamic Topography (MDT) maps, both referenced over a 20-year period in the Ssalto/Duacs 2014 version [*Duacs/AVISO+*, 2015]. The improved data processing used in DT14 provides a better description of mesoscale activity than previously distributed products [*Capet et al.*, 2014; *Pujol et al.*, 2016].

Most (Deleted: ~~of the~~)published studies, which also include previous (Replaced: ~~delopments~~ replaced with: developments) of the current method [*Chaigneau et al.*, 2011; *Pegliasco et al.*, 2015], (Added: have)applied an eddy-detection algorithm applied to SLA. This was essentially to avoid errors due to the imprecision of the definition of the Earth geoid. Recently, the availability of the latest version of MDT (MDT CNES-CLS13, [*Rio et al.*, 2014]), calculated from a 20-year average (1993-2012) of altimetry data and a geoid

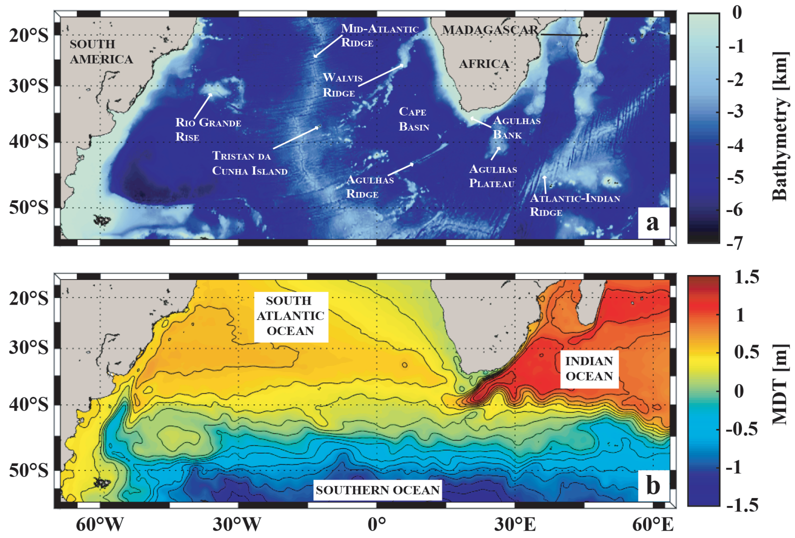

Figure 1. Study domain and a) bathymetry from the ETOPO2 data set [*Smith and Sandwell*, 1997] and b) Mean Dynamic Topography (MDT, [*Duacs/AVISO+*, 2014]) with the main currents indicated.

obtained by correcting the Gravity and Ocean Circulation Experiment (GOCE) model with dynamic height and velocity estimates derived from in(Replaced: ~~-~~ replaced with:)situ observations [*Rio et al.*, 2011, 2014] (Replaced: ~~allows for~~ replaced with: provides) a better estimate of the geopotential surface height of the ocean(Added: ,) which significantly improves ADT and the associated ocean dynamics [*Rio et al.*, 2014]. (Replaced: ~~As~~ replaced with: Like) *Halo et al.* [2014], we choose to use ADT instead of SLA maps because the latter are strongly affected by the position and displacement of large SSH gradients associated with intense currents (Replaced: ~~as~~ replaced with: and) well as quasi-stationary meanders and eddies, all included in MDT as shown in Figure 1b. This is particularly true for the Agulhas Current system. In fact, small (Replaced: ~~displacements~~ replaced with: shifts) relative to (Deleted: ~~the~~)average current (Deleted: ~~s~~) positions can generate artificial dipoles of positive and negative SLA. These dipoles are identified as two eddies in SLA whereas they are not detected in ADT. In addition, ADT is directly associated with important physical variables such as ocean currents and the geostrophic stream function.

2.2 The Ocean Eddy Detection and Tracking Algorithms (TOEddies)

This eddy detection algorithm is an evolution of the method proposed and developed by *Chaigneau et al.* [2008, 2009]. It is based on the key assumption that for geostrophic eddies, (Added: the)streamlines correspond to the closed contours of Sea Surface Height (SSH). The eddy detection algorithm is a two-step process: it identifies the occurrence (Deleted: ~~s~~) of eddies before deriving their trajectories.

First and foremost, the method identifies the local extrema (maxima and minima) of ADT as possible eddy centers. Then, it looks for the outermost closed ADT contours around each extremum. The module of the ADT difference between the extremum and this contour defines the detected eddy amplitude which is considered as a proxy of the eddy (surface) signature. *Cipollone et al.* [2017] showed that two close (Deleted: ~~-by~~) extrema can be dependent (Replaced: ~~thus they~~ replaced with: and thus) defined a minimum distance between extrema (Replaced: ~~for them to be~~ replaced with: so that they are) considered as possible eddy centers. In this study(Added: ,) we introduced as a parameter of the eddy detection method, a minimum threshold for the amplitude of (Added: the)eddy extrema. This ensures that a detected extremum can be considered (Added: as)an eddy center. Extrema associated with an amplitude below the threshold will not be a constraint for the detection of the outermost closed ADT contours associated with others extrema.

This parameter (the eddy amplitude threshold) can be interpreted as (Added: an)eddy "persistence", a notion of topological simplification introduced by *Edelsbrunner et al.* [2002] and *Edelsbrunner and Harer* [2010] which has (Replaced: ~~extensively~~ replaced with: been widely) used since [e.g. *Tierny et al.*, 2018]. The persistence criterion by reducing the number of extrema (Replaced: ~~is intended~~ replaced with: aims) to avoid the over-representation of dynamically insignificant structures (Replaced: ~~as~~ replaced with: because) it should prevent the artificial separation of a large eddy into two or more smaller elements. Therefore, in the following, the amplitude threshold parameter will be (Replaced: ~~referred to as the~~ replaced with: called) "persistence" to distinguish it from the minimum amplitude criterion that has been widely used in the literature [e.g. *Chelton et al.*, 2011]. *Faghmous et al.* [2015] showed that the minimum amplitude criterion, with its typical value of 1 cm, could lead to (Replaced: ~~a~~ replaced with: the) loss of significant structures. A sensitivity test on eddy persistence is presented in Table(Replaced: ~~-T1 in the supplementary material~~ replaced with: A.1 of the Appendix) according to the method presented in Section(Replaced: ~~3~~ replaced with: **??**.). It shows that a non-zero value for the persistence parameter (Added: (set to 1 mm))increases the number of structures as well as the ability of our detection method to define eddies. However, a further increase in the persistence parameter value does not show significant improvements in (Added: the)eddy detection capability. This is why we have set this parameter value to 1 mm. Note that this value, which acts somewhat (Replaced: ~~as~~ replaced with: like) a low(Replaced: ~~-~~ replaced with: p)ass filter, is considerably smaller than the (Added: resolution of)1 to 2 cm defined in the literature as the nominal resolution of satellite altimetry.

The detected ADT extrema that pass the persistence threshold are each identified as the center of an eddy if there is at least one (Deleted: ~~single~~)closed ADT contour containing only one local extreme and including at least 4 connected grid points. The size of each eddy is then characterized by two distinct radii. The equivalent outermost radius, $\mathrm{R_{out}}$, (Replaced: ~~that~~ replaced with: which) corresponds to the radius of a disk having the same area ($\mathrm{A_{out}}$) as that (Replaced: ~~enclosed~~ replaced with: delimited) by the outermost closed contour. (Replaced: ~~T~~ replaced with: I)ts value is given by the equation:

$$\mathrm{R_{out}} = \sqrt{\frac{A_{out}}{\pi}} \tag{1}$$

However, the outermost (Added: closed contour)is often (Replaced: ~~highly~~ replaced with: strongly) distorted by the surrounding flow and interactions with others mesoscale (Replaced: ~~features~~ replaced with: structures). For this reason, we also used, as a reference variable for the method, the contour (Replaced: ~~which corresponds~~ replaced with: corresponding) to the ADT contour along which the mean azimuthal geostrophic velocity is maximum ($\mathrm{V_{max}}$). This limit, called (Replaced: ~~characteristic contour~~ replaced with: the "characteristic contour") in this study, tends to be more robust and coherent in time than the outermost contour. We (Deleted: ~~have~~)then defined the maximum speed radius, $\mathrm{R_{Vmax}}$, associated (Replaced: ~~to~~ replaced with: with) the area (Replaced: ~~enclosed~~ replaced with: delimited) by the characteristic contour. $\mathrm{R_{Vmax}}$ is always smaller or equal to $\mathrm{R_{out}}$. It characterizes the eddy core and allows (Deleted: ~~for~~)easy comparisons with in(Replaced: ~~-~~ replaced with:)situ (Replaced: ~~mearsurements~~ replaced with: measurements) such as ADCP transects or drifter (Deleted: ~~s~~) trajectories [*Mkhinini et al.*, 2014; *Ioannou et al.*, 2017; *Garreau et al.*, submitted]. The accuracy of each eddy center (associated with a local ADT extremum) is limited by that of the ADT field defined at (Deleted:

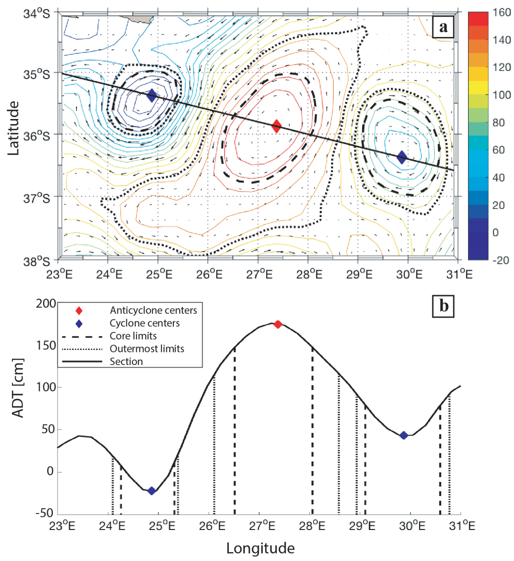

Figure 2. Example of eddies detected near the Agulhas Current on 23 March 2000. Two cyclones and one anticyclone are shown in a) an ADT map and b) in terms of ADT amplitude along a section crossing the extrema of the eddies detected in (a). For each eddy, the ADT contours where the azimuthal speed is maximum (eddy core limit - dashed lines) and the outermost closed contour (eddy outer eddy limit - dotted line) are shown. ADT isolines with 10 cm intervals and the geostrophic velocity vectors distributed by AVISO are superimposed in (a).

~~1/4°~~)horizontal resolution(Added: of 1/4°). Because of this precision limit, we ch (Deleted: ~~o~~)ose to use the centroid of the area associated with the eddy core as the center of each structure. Indeed, this variable is less affected by the ADT resolution. An example of the two boundaries (Replaced: ~~for~~ replaced with: of) two cyclones and an anticyclone and their eddy centers is (Replaced: ~~illustrated~~ replaced with: shown) in Figure 2.

The vortex surface Rossby Number (Ro) is used to compare (Replaced: ~~the~~ replaced with: eddy) characteristics (Deleted: ~~of the eddies~~)in different regions [e.g. *Chelton et al.*, 2011; *Mkhinini et al.*, 2014; *Le Vu et al.*, 2018], (Replaced: ~~which~~ replaced with: as it) is a proxy of the surface intensity of the dynamic core (equation 2, where f is the Coriolis parameter).

$$Ro = \frac{V_{max}}{f R_{V max}} \qquad (2)$$

In a second step of the eddy detection method, a complete and continuous set of eddy trajectories is recovered by following the paths of the eddies between successive ADT maps. Taking advantage of daily AVISO fields the method relies on the fact that mesoscale eddies move slowly (displacements of less than 10 km/day, see also *Chelton et al.* [2011]) relative to their radii (Replaced: ~~which~~ replaced with: that) typically (Replaced: ~~span~~ replaced with: extend) from 20 to 200 km [*Carton*, 2001]. This ensures that the areas covered by the same eddy for two consecutive days overlap. (Replaced: ~~Such~~ replaced with: This) overlap can be used to track eddies [*Pegliasco et al.*, 2015]. We use the characteristic contour (R_{Vmax}), less distorted than the outermost contour, to define the surface of the eddy core. However, in sporadic cases, the eddy surfaces defined by R_{Vmax} for two consecutive days do not overlap. Hence, we set the method to check in parallel the overlap (Deleted: ~~ping~~) of the eddy surface defined by the outermost contour. To avoid (Replaced: ~~spurious association of eddies, a minimum overlapping percentage~~ replaced with: false eddy associations, a minimum percentage of overlap) is required when considering this (Replaced: ~~wider~~ replaced with: larger) eddy surface. This overlap threshold, which is calculated as the ratio of the overlap area to the area of the smaller of the two eddies, provides robust eddy tracking (Figure 3a). Indeed, assuming a small circular eddy with a radius of 20 km moving at a speed of 10 km/day, 73% of its surface will overlap for two days. Therefore, the threshold should be less than 70%. Unfortunately, due to the small number of long(Replaced: ~~-lived~~ replaced with: life) trajectories identified from (Replaced: ~~drifters (see Section 3),~~ replaced with: drifting buoys (see Section **??**),) this parameter could not be tested quantitatively. Instead, qualitative trajectory inspections using different percentages of the overlap threshold (0, 25 and 50%) were undertaken. Due to the need for confidence in the method and the fact that comparisons between drifting buoys and (Replaced: ~~altimetry derived eddy trajectories~~ replaced with: eddy trajectories derived from altimetry) showed (Deleted: ~~some~~)suspicious trajectories using small (Replaced: ~~values of the overlap threshold, the 50% value is chosen. As already documented by some authors~~ replaced with: overlap threshold values, the value of 50% was chosen. As some authors have already documented) [e.g., *Chaigneau et al.*, 2008; *Chelton et al.*, 2011; *Faghmous et al.*, 2015; *Le Vu et al.*, 2018], eddies can disappear from altimetry maps for several days as a consequence of the heterogeneous distribution of the altimetr(Replaced: ~~ie~~ replaced with: y) tracks. To take into account this possible lack of detection, an eddy, which has no parents in the previous time step or children in

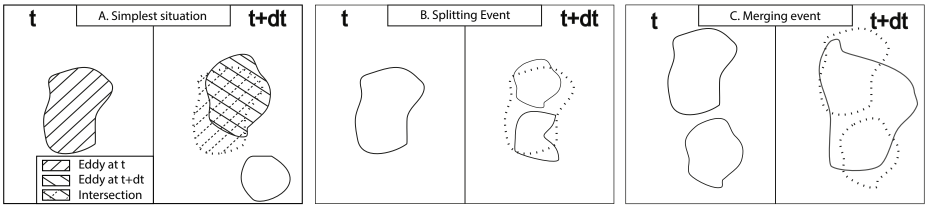

Figure 3. Schematic diagram of the eddy tracking step of the algorithm. a) Simplest situation where a single eddy is identified at the two different time intervals, t and $t + dt$. The area of the two eddy occurrences and their overlapping surface are shown, the latter in the form of a hatched surface. b) Splitting event. c) Merging event. Although the overlap threshold is applied in b) and c), these areas have not been represented to ensure readability of the figures.

the following (Replaced: ~~one~~ replaced with: time step), is allowed to continue to exist if its disappearance does not last (Replaced: ~~longer~~ replaced with: more) than 5 consecutive days.

Nonlinear interactions between distinct eddies or between eddies and topography are some of the processes that can induce the (Deleted: ~~ir~~) splitting or merging(Added: of eddies). These processes have been both theoretically supported [e.g., *Melander et al.*, 1988; *Simmons and Nof*, 2000; *Drijfhout*, 2003] and observed [e.g., *Cresswell*, 1982; *Schultz Tokos et al.*, 1994; *Isoda*, 1994; *Sangrà et al.*, 2005; *Garreau et al.*, submitted]. The TOEddies algorithm belongs to the very few eddy detection and tracking algorithms [*Yi et al.*, 2014; *Matsuoka et al.*, 2016; *Qiu-Yang et al.*, 2016; *Le Vu et al.*, 2018] that (Replaced: ~~takes~~ replaced with: consider) both processes (Deleted: ~~into account~~). It (Replaced: ~~associates~~ replaced with: combines) the separation of a large eddy with two or more smaller eddies in the (Deleted: ~~splitting~~)case (Added: of splitting)(see Figure 3b), and relates the coalescence of two or more small eddies into a larger eddy in the case of merging (see Figure 3c).

To take (Replaced: ~~into account these processes~~ replaced with: these processes into account), a relationship tree is created associating each eddy (Replaced: ~~to~~ replaced with: with) its potentials parent (Deleted: ~~(~~)s (Deleted: ~~)~~) and child (Deleted: ~~(~~)ren (Deleted: ~~)~~). Independent eddy trajectory segments are constructed by scanning this tree. (Replaced: ~~They~~ replaced with: These segments) are trajectories (Replaced: ~~which~~ replaced with: that) link (Added: the)eddy positions between (Added: the)merging and splitting events.

Therefore, each segment begins either after the detection of a new eddy, or after the merging of two eddies or the splitting of (Replaced: ~~one~~ replaced with: an) eddy into two or more smaller eddies, and ends the time step before a new eddy-eddy interaction or when the eddy disappears from the altimetry maps.

The next step is to combine these segments to reconstruct the main eddy trajectories. (Replaced: ~~For that~~ replaced with: To do this), the method (Added: first) evaluates (Deleted: ~~, beforehand,~~) the overlap of (Added: the)eddy surfaces associated (Deleted: ~~to~~)characteristic contours (A_{Vmax}). In many case(Added: s), only two segments can be associated. From their (Replaced: ~~assemblage~~ replaced with: assembling) a main eddy trajectory is defined. In (Replaced: ~~a following~~ replaced with: the next) step, the method (Replaced: ~~looks~~ replaced with: searches) for (Replaced: ~~the overlap of~~ replaced with: overlapping) eddy surfaces associated with $\mathrm{R_{out}}$. This step is used to define trajectories that split from or merge with the eddy main trajectory. During eddy merging and splitting events, an eddy defined by the surfaces associated with $\mathrm{R_{Vmax}}$ can be (Replaced: ~~linked~~ replaced with: associated) with more than one segment. In these cases, we use a cost function to identify the main eddy trajectories. (Replaced: ~~The use of~~ replaced with: Using) a cost function to define eddy trajectories is a relatively standard approach [e.g. *Penven et al.*, 2005; *Chaigneau et al.*, 2008, 2009; *Frenger et al.*, 2015; *Le Vu et al.*, 2018]. The cost function we (Deleted: ~~have~~)defined (equation 3) takes into account the distance between (Added: the)successive eddies and the change in (Replaced: ~~surface properties of the eddy core~~ replaced with: eddy core surface properties) (i.e., within the $\mathrm{R_{Vmax}}$ limit). (Replaced: ~~The i~~ replaced with: I)ndependent segments that minimize the cost function are linked together. The resulting long series of segments is identified as the main eddy trajectory. The remaining trajectories are classified as the result of an eddy splitting from the main trajectory or an eddy merging with the main trajectory.

$$CF = \sqrt{\left(\frac{\Delta Center - \overline{\Delta Center}}{\sigma_{\Delta Center}}\right)^2 + \left(\frac{\Delta Ro - \overline{\Delta Ro}}{\sigma_{\Delta Ro}}\right)^2 + \left(\frac{\Delta R_{Vmax} - \overline{\Delta R_{Vmax}}}{\sigma_{\Delta R_{Vmax}}}\right)^2} \qquad (3)$$

The cost function we used ((Replaced: ~~dubbed as~~ replaced with: called) CF in the following) is presented in equation 3 where, for a difference $\Delta\alpha$ of the generic variable α between two independent segments, $\overline{\Delta\alpha}$ and $\sigma_{\Delta\alpha}$ denote, respectively, the mean and the standard deviation of the differences. They are calculated between all pairs of a parent eddy associated with a single child eddy. The variables we used in (Replaced: ~~the~~

~~definition of~~ replaced with: defining) the cost function are based on the work (Replaced: ~~by~~ replaced with: of) *Le Vu et al.* [2018]. In addition, we prescribed (Deleted: ~~the estimate of both,~~)the mean and the standard deviation (Added: estimates)of the variables used in the cost function following *Pegliasco et al.* [2015] to ensure similar ranges of variation for every variable (Deleted: ~~in order~~)to assign them the same weight.

In (Replaced: ~~an attempt~~ replaced with: order) to reduce the effect of spurious variations in the gridded ADT product, the values used in CF are averaged over (Deleted: ~~either~~)the last (Replaced: ~~seven or~~ replaced with: or the)first seven days of each independent segment in the case of eddy merging and splitting(Added: ,) respectively. In this way, the CF can, for example, identify two trajectories that merge for only few time steps before splitting again. In this case, this event is identified as an interaction instead of a real merging followed by a splitting. This is close to the neutral interactions presented in *Le Vu et al.* [2018] with (Replaced: ~~the~~ replaced with: an) interaction period (Replaced: ~~fixed to~~ replaced with: set at) 5 days. To limit the number of short (Replaced: ~~lived~~ replaced with: life) segments that connect (Added: the)trajectories or increase the number of eddy-eddy interactions, each independent segment must last (Deleted: ~~for~~)more than 4 weeks to be taken into account. This ensures that the segments of a trajectory are consistent over a relatively long period of time.

Taking into account eddy merging and splitting, the meaning of an eddy trajectory (Deleted: ~~changes~~)radically (Replaced: ~~from~~ replaced with: changes) the traditional view of mesoscale eddies (Replaced: ~~that move~~ replaced with: moving) as isolated and coherent structures from their formation (Replaced: ~~area~~ replaced with: zone) to their dissipation (Replaced: ~~area~~ replaced with: zone). This is why we propose here to characterize the evolution of these structures not in terms of eddies, but by a network of trajectories. Such a network is composed of several branches identified as independent segments that begin either with a merging or splitting event or with the formation of a new structure(Added: ,) and end with another merging or splitting event or with the disappearance of the structure in the altimetry maps.

To match the in situ observation of isolated eddies with the associated trajectory network, we propose assigning an (Deleted: ~~d~~) order to each segment of a main trajectory as shown in Figure 4. In this formalism, the “order 0” of the trajectory network is the main trajectory identified by applying the CF for each occurrence of merging and splitting.

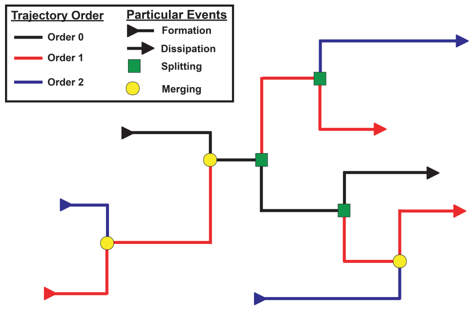

Figure 4. Schematic of a simple network of trajectories up to order 2. This network is characterized by 4 formations, 4 disappearances, and 3 merging and splitting events. With each merging and splitting, the cost function is applied to follow the main trajectory by associating a segment with a higher order.

With “order 1”, we assign (Deleted: ~~the~~)segments that are linked to the main trajectory either (Replaced: ~~via~~ replaced with: by) an eddy splitting or an eddy merging. Similarly, the “order 2” refers to (Deleted: ~~the~~)segments that are associated with eddy merging or splitting with (Deleted: ~~the~~)“order 1” trajectories, etc. This recursive classification in ordered trajectories continues until no new orders are detected. (Replaced: ~~Every~~ replaced with: Each) network is therefore associated with an order n of trajectories. The “order 0” of each network of trajectories is defined according to the target of the study as, for example, the assessment of the origin and fate of a mesoscale eddy (Replaced: ~~observed~~ replaced with: identified) by in situ observations or a global view of mesoscale eddies formed in a particular region of the ocean, such as (Added: the)Agulhas Rings.

2.3 The AVISO+ Mesoscale Eddy Trajectory Atlas

Chelton et al. [2011] is the most publicly available (Deleted: ~~cited~~)atlas (Added: cited)for mesoscale eddies automatically defined from satellite altimetry data. A new version of this algorithm has been implemented by *Schlax and Chelton* [2016] which is used by SSALTO/DUACS to produce the Mesoscale Eddy Trajectory Atlas (hereafter META2017) [*Duacs/AVISO+*, 2017] distributed by AVISO+ (http://www.aviso.altimetry.fr/) with support from CNES, in collaboration with (Deleted: ~~the~~)Oregon State University with support from NASA.

The META2017 detection method is based on the geographical properties of the “two-sat-merged” SLA maps after (Deleted: ~~the~~)application of a spatial high-pass filter.

The META2017 algorithm identifies anticyclonic (cyclonic) eddies by locating the pixel at a local maximum (minimum) of SLA and successively finding all neighboring pixels with SLA values above (below) a sequence of decreasing (increasing) thresholds following the "growing method" of *Williams et al.* [2011]. This "growth" of the eddy structure continues until one of the five criteria defining a compact and coherent structure is violated. The five criteria used are chosen to generate eddies statistically similar to those obtained by *Chelton et al.* [2011]. Eddies (Replaced: ~~whose~~ replaced with: with an)amplitude (Replaced: ~~is~~ replaced with: of) less than 1 cm are not (Replaced: ~~taken into account~~ replaced with: included) in META2017. This algorithm is described in detail in *Schlax and Chelton* [2016] and the eddy atlas in *Duacs/AVISO+* [2017].

One of the main difference(Added: s) between TOEddies and (Deleted: ~~the~~)META2017 algorithms (Replaced: ~~lies in the eddy-tracking~~ replaced with: lies in the eddy tracking) step. META2017 applies a cost function to (Added: the)eddies in (Replaced: ~~subsequent~~ replaced with: the successive) maps in an (Replaced: ~~elliptic~~ replaced with: elliptical) search area whose size depends on latitude. TOEddies, instead, requires eddy areas to overlap. The META2017 cost function compares the amplitude and position of the identified eddies with those of the next time step. It then selects only (Replaced: ~~a single~~ replaced with: one) structure to define the trajectory of the eddy. It therefore (Replaced: ~~considers neither~~ replaced with: does not take into account) eddy merging nor eddy splitting processes. In META2017, only eddies of at least 4 weeks (Deleted: ~~old~~)are documented.

2.4 "Loopers" recovered from Surface Drifters

The robustness of the method and the related parameter (Deleted: ~~s~~) choices were evaluated by comparing our results with independent in(Replaced: ~~-~~ replaced with:)situ data. To do this, we used the eddies identified by *Lumpkin* [2016] (hereafter LU16) from the Global Drifter Program quality-controlled surface drifters data [*Lumpkin and Pazos*, 2007] over the world ocean from February 1979 to July 2017 (http://www.aoml.noaa.gov/phod/loopers/index.php). In LU16 (Deleted: ~~-~~), eddies are automatically identified as "looping" trajectories of drifters buoys reconstructed from the 4 positions they sen(Replaced: ~~t~~ replaced with: d) each day. To do this, the methodology initially introduced by *Veneziani et al.* [2004] and (Deleted: ~~further~~)developed by *Griffa et al.* [2008] and LU16 is used. In this method, the spin Ω of each trajectory that can be related to the vorticity of the Eulerian fluid field for a particle

(Replaced: ~~in solid-body rotation~~ replaced with: following the rotation of a solid body) [*Veneziani et al.*, 2004] is computed at each position. (Replaced: ~~By u~~ replaced with: U)sing the properties of circular motion, we can estimate both the period and (Deleted: ~~the~~)radius of (Replaced: ~~such looping~~ replaced with: these loop) trajectories. We refer to LU16 for a complete description of the method.

It should be noted here that LU16 underestimates the total number of eddies because it only accounts for (Deleted: ~~those~~)eddies captured by the (Replaced: ~~sparse~~ replaced with: small) number of drifting buoys deployed in the ocean. In addition, LU16 estimates only the radius of (Replaced: ~~each drifter's loop,~~ replaced with: the loops of each drifter,) which may be different (essentially smaller) than the actual radius of the (Deleted: ~~sampled~~)eddy(Added: sampled). Indeed, it (Replaced: ~~was~~ replaced with: has been) shown by *Chaigneau and Pizarro* [2005](Added: , by) comparing (Replaced: ~~eddy~~ replaced with: the eddies) detected from altimetry against drifting buoys(Added: ,) and by *Pegliasco et al.* [2015](Replaced: ~~against lagrangian~~ replaced with: , with Lagrangian) profiling floats that, (Replaced: ~~i~~ replaced with: o)n average, these instruments sample the eddy at 2/3 of the R_{out} which correspond(Added: s) to a random sampling of a disk (Replaced: ~~of~~ replaced with: with a) radius equal to R_{out}. Therefore, to avoid erroneous comparisons of eddy radii, only (Deleted: ~~the~~)LU16 eddy(Replaced: ~~-~~ replaced with:)center positions are used. We followed LU16 to evaluate such a center(Added: : it is defined) as the mean cent(Replaced: ~~ral~~ replaced with: er) position of the buoy's (Added: looping)trajectory during a (Replaced: ~~period of rotation~~ replaced with: rotation period). The instantaneous radius of each eddy detected by LU16 is computed as the distance between the estimated position of the eddy(Replaced: ~~-~~ replaced with:)center and the (Deleted: ~~associated~~)position of the drifter along its loop.

3 Validation and Comparison of Eddies Datasets

3.1 The Validation Approach

For validation purposes, a daily (Replaced: ~~colocalization~~ replaced with: collocation) was performed between the five eddy datasets listed in Table 1 in the South Atlantic - Southeast Indian geographical domain [70°W-65°E; 55°S-15°S] during the period 1 January 1993 to 31 December 2016. Only LU16 eddies whose (Deleted: ~~eddy~~)center is at least (Deleted: ~~at a distance of~~)5° (Added: away)from the (Replaced: ~~boundaries~~ replaced with: limits) of the geographical domain are taken into account. Indeed, eddies close to the limits of the domain may not be detected by TOEddies. In what follows, LU16 will be the reference dataset. Within this framework, only (Added: the) trajectories of drogued surface drifters for which (Added: a position of)an eddy center (Deleted: ~~position~~)could be estimated and whose radius is (Replaced: ~~smaller~~ replaced with: less) than 300 km are chosen, which constitutes a reasonable upper limit for mesoscale ocean eddies [*Carton*, 2001].

This selection results in 38503 anticyclonic and 40251 cyclonic eddy centers identified by LU16 in the study area. Only surface drifters trapped in a structure for more than a week are used here for the validation of eddy trajectories. Only 431 anticyclonic and 414 cyclonic LU16 trajectories last (Added: for)more than seven weeks in the region. This number is relatively small because we (Added: only)took into account (Deleted: ~~only~~)LU16 loopers associated (Replaced: ~~to~~ replaced with: with) radii (Replaced: ~~smaller~~ replaced with: less) than 300 km. (Replaced: ~~As a consequence~~ replaced with: Therefore), the LU16 trajectories used in this study are shorter than (Deleted: ~~those~~)originally estimated.

In Figure 5 the number of LU16 eddies available for cross detection are plotted according to their radii that we (Deleted: ~~have~~)recalculated. The resulting LU16 mean radii are between 0 and 10 km for anticyclones and (Added: between)10 and 20 km for cyclones. The number of eddies in each size interval decreases as (Replaced: ~~structure~~ replaced with: the) size (Added: of the structure)increases. The median is about 25 km for both types of eddies. 90% of cyclones have a radius (Deleted: ~~of~~)less than 56 km and 90% of anticyclones have a radius (Deleted: ~~of~~)less than 74 km. (Replaced: ~~Less~~ replaced with: Fewer) than 1% of cyclones and 2% of anticyclones have a radius greater than 100 km.

As (Deleted: ~~previously~~)mentioned(Added: earlier), the estimated radii (Replaced: ~~from~~ replaced with: of) the LU16 loopers cannot be an estimate of the true size of mesoscale eddies(Added: ,) as surface drifters loop along circles that are smaller than (Added: the)eddy cores. However, they can be used to (Replaced: ~~set~~ replaced with: define) a minimal size for mesoscale eddies. Half of the LU16 distributions have radii (Replaced: ~~larger~~ replaced with: greater) than 25 km(Added: ,) which corresponds approximately to the pixel size of 1/4° horizontal resolution in altimetry gridded products. It is therefore rea-

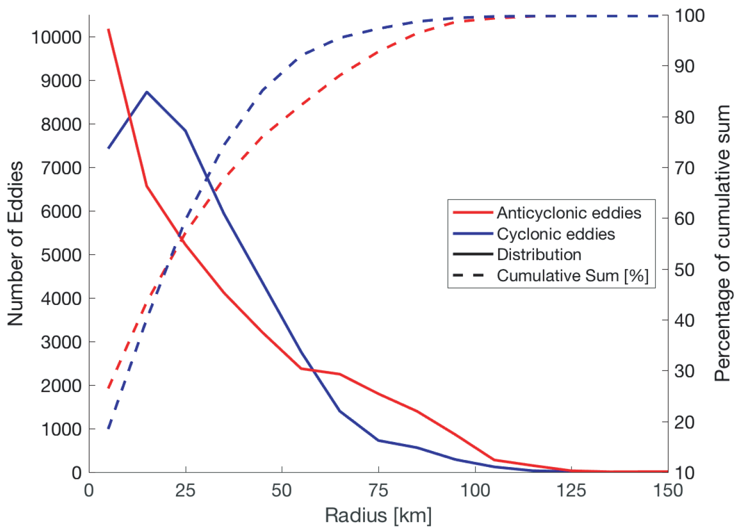

Figure 5. Number of eddies (on the ordinate) identified from surface drifting buoys by *Lumpkin* [2016] and used to validate the robustness of the eddies identified by the TOEddies algorithm shown as function of their radii (on the abscissa). The radii are sampled every 10 km. These numbers are computed separately for anticyclonic and cyclonic eddies.

sonable to use LU16 loopers to validate the eddies detected in the altimetry fields. Since only a small fraction of the LU16 eddies have a radius greater than 100 km, we (Added: have)set the maximum radius to be (Replaced: ~~considered~~ replaced with: taken into account)to this value.

For validation, we consider that two eddies are co-located (i.e, (Added: a)valid cross-detection) if (Replaced: ~~a~~ replaced with: the) center of (Added: a)LU16 eddy falls in the area occupied by an eddy of the same sign detected by one of the (Replaced: ~~algorithms based on altimetry~~ replaced with: altimetry-based algorithms). An example of this type of matching is shown in Figure 6. For datasets that do not explicitly provide the eddy contour (e.g., META(Added: 20)17), a correspondence exists if the (Replaced: ~~LU16 eddy center and~~ replaced with: center of one LU16 eddy and the center of one eddy) that in the other dataset is (Replaced: ~~at~~ replaced with: within) a distance smaller than the eddy radius defined in (Replaced: ~~the atlas derived from altimetry~~ replaced with: such dataset).

(Replaced: ~~The~~ replaced with: We implemented the) collocation with LU16 loopers (Deleted: ~~is applied~~)to the datasets listed in Table 1. The first four datasets correspond to the TOEddies detection algorithm applied to the two different altimetry maps (SLA and

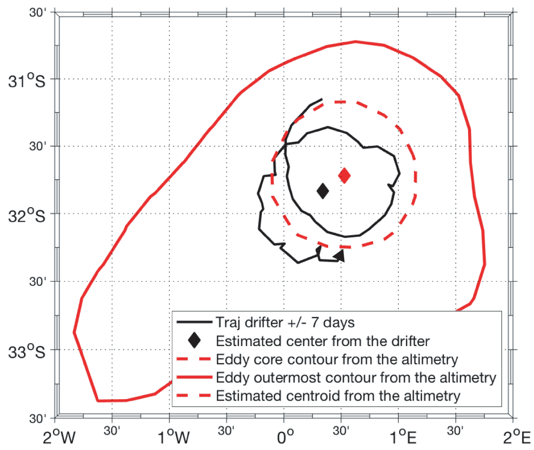

Figure 6. Example of cross-detection of eddies for 12 December 2012 where an eddy identified from a surface drifter trajectory by LU16 (in black with a diamond symbol locating its center) and an anticyclone detected in the TOEddies Atlas (red contours for its outer limit and its maximum speed core) overlap.

ADT) and parameter thresholds. The first three letters of these datasets indicate the type of map used as input. Moreover, (Replaced: ~~whereas~~ replaced with: while) in TOEddies we apply a (Added: 4-week)threshold (Deleted: ~~of 4 weeks~~) on the life (Deleted: ~~time~~) of eddy segments that filters out segments associated with short-lived eddies, the suffix "_raw" is added when this filtering is not applied. The suffix "_rad" refers to the results of (Deleted: ~~the~~)LU16-TOEddies collocation performed in the same (Replaced: ~~way~~ replaced with: manner) as (Deleted: ~~for~~)LU16-META(Added: 20)17, i.e. using the eddy radius instead of the eddy area criterion.

3.2 Validation of the Eddy Detection and Tracking Algorithms

In the following (Replaced: ~~the~~ replaced with: we summarize the main) results of the cross-validation between LU16 and the different eddy satellite altimetry databases listed in (Replaced: ~~Table 1 are discussed. Table 2 lists the number of eddies identified in each dataset and their detection efficiency expressed as percentage of the total number of collocation with LU16 eddies. To assess the skill of the method and provide quantitative comparisons between the various eddy datasets, a matching percentages is computed. It represents the proportion of each polarity of the LU16 eddies that were successfully cross-detected with eddies of the same polarity in each dataset (Table 2). The cross-detection errors are also defined as mismatches in eddy polarity or when several eddies detected by~~

Table 1. Parameters of the 6 datasets tested against the independent LU16 eddy atlas derived from surface drifter buoys. Each row corresponds to a different dataset for which the version and the type of satellite altimetry maps used for the detection is specified. The suffix "_raw" is added when the 4-week threshold on lifetime eddy segments is not applied. The suffix "_rad" refers to the results of the LU16-TOEddies collocation performed using the eddy radius instead of the eddy area criterion. N/A (not applicable) is added when a parameter is not relevant for a dataset.

Dataset Name	Persistence or Minimum Amplitude [mm]	Minimum surface [%]	Lifetime [week]
SLA_raw	1	N/A	N/A
ADT_raw	1	N/A	N/A
TOEddies	1	50	4
TOEddies_rad	1	50	4
META2017	10	N/A	4

~~altimetry were assigned to the same LU16 eddy.~~ replaced with: Table 1, as well as the different threshold parameters and a thorough comparison with the META2017 atlas. Details of validation and comparisons are discussed in the Appendix.)

(Deleted: ~~The TOEddies detection algorithm was tested on both, SLA and ADT maps (without applying any threshold on eddy life-span) in order to evaluate the most relevant altimetry dataset for automatic eddy-detection. Table 2 shows that the TOEddies algorithm (refered to SLA_raw and ADT_raw) detects 34% (36%) more anticyclonic (cyclonic) eddies when SLA instead of ADT maps are used. The total area occupied by eddies derived from SLA is larger than that resulting from the use of the ADT field. This area exceeds by 31% (50%) when referring to the eddy contour defined by R_{Vmax} for anticyclones (cyclones) and by 48% (65%) when the eddy limiting contour is defined by R_{out}.~~)

(Deleted: ~~When comparing the effectiveness of the results with LU16 and using the outer contour as eddy edge (Table 2), the ADT maps show a slightly better agreement for anticyclones (by about 2%) while the SLA maps give a somewhat better result for cyclones (by about 3%). On the other hand, when the contour of maximum velocity is taken as eddy boundary, the differences in detection efficiency between the SLA and ADT~~

Table 2. Detection and collocation matching statistics with LU16 eddies. "max" refers to the eddy contours associated with their maximum speed while "out" refers to their outer contours. The percentages indicate the proportions of eddies by polarity as defined in LU16. Anti and Cyclo mean, respectively, anticyclones and cyclones. N/A (not applicable) is added when a parameter is not relevant for a dataset.

Dataset	Number Eddies anti/cyclo [10^6]	Sum Area max anti/cyclo [10^{10} km^2]	Sum Area out anti/cyclo [10^{10} km^2]	Match Anti max / out [%]	Mismatch Anti max / out [%]	Match Cyclo max / out [%]	Mismatch Cyclo max / out [%]
SLA_raw	4.3 / 4.5	4.3 / 4.2	7.7 / 7.6	62 / 69	2 / 4	72 / 78	1 / 2
ADT_raw	3.2 / 3.3	3.2 / 2.8	5.2 / 4.6	66 / 71	2 / 3	71 / 75	1 / 2
TOEddies	2.4 / 2.5	2.8 / 2.5	4.7 / 4.2	63 / 67	2 / 3	65 / 69	1 / 2
TOEddies_rad	2.4 / 2.5	2.8 / 2.5	4.7 / 4.2	60 / 63	1 / 3	64 / 65	1 / 4
META2017	1.8 / 1.8	4.1 / 4.1	N/A / N/A	50 / N/A	3 / N/A	53 / N/A	3 / N/A

maps decrease in the case of cyclones while, for anticyclones, the ADT shows better results (4% more effective).)

(Deleted: To validate the robustness of the TOEddies threshold requiring a minimum longevity of 4 weeks for a trajectory segment, the results of ADT_raw and TOEddies are compared. Table 2 shows that such a threshold reduces both the number and total extent of eddies. The number of eddies decreases by 25% and the total area they occupy by 10%. This is mainly due to the fact that the threshold on the segment life-span criterion reduces the number of small eddies. In terms of validation compared to LU16, the number of collocations decreases for both cyclones and anticyclones when the time threshold is used (Table 2). This is particularly true for cyclones. Note here that the higher matching of the algorithm, independently of the time threshold or the base altimetry field, is obtained for the eddy perimeters defined by the outer contour albeit there is a slight increase in errors.)

(Deleted: As META17 is probably the most widely used eddy atlas derived from satellite altimetry, in order to have another independent measure of the performance of our algorithm, we quantitatively compare META17 and TOEddies global statistics and skills. Table 2 suggests that META17 identify 25% fewer eddies but their overall extent is 41% larger. Figure 7 shows the statistical distribution of META17 and TOEddies radii. The distribution maximum is positioned at about 40 km for TOEddies and 60 km for META17. A clear difference between cyclones and anticyclones appears in TOEddies where cyclones are, on average, smaller than anticyclones. This difference is also noticeable in META17, but less marked. In TOEddies, less than 1% of the eddies have a radius greater than 140 km while it corresponds to 5% of the structures for META17.)

(Deleted: In order to compare the size of the eddies detected by satellite altimetry with an independent variable linked to the mesoscale ocean dynamics, we estimated the first Rossby baroclinic radius (L_R). L_R characterizes regionally the size of the long-living eddies in the open ocean. L_R mean value was calculated using the definition of citetChelton:1998 and the seven-year averaged (i.e. 2005 to 2012) World Ocean Database citepBoyer:2013. The resulting value is represented by the vertical dotted line in Figure 7. The shaded area represents L_R percentiles 10 and 90. This figure shows that TOEddies identifies structures that have a size comparable to L_R (around 60% of TOEddies radii fall within

~~the percentile range L_R 10 - 90) while this is not the case for META17, for which less than 20% of the radii fall within this interval.~~)

(Added: All datasets tested (Table 1) show both, a decrease in error and an increase in detection efficiency for LU16 eddies with large radii (see Table 2. This is most likely due both to the limited spatial resolution of satellite altimetry and its limited ability to capture small structures [e.g. *Chelton et al.*, 2011] but also to the lower probability that drifting buoys are captured in small eddies rather than in large eddies. However, it should also be noted that LU16 eddy radii may provide an underestimate of the actual size of structures. Indeed, drifting buoys are drawn by the movement of the upper ocean at different distances from the center of the eddy and they do not necessarily move along the outer eddy edge of the eddy or along its maximum velocity. Indeed, it has been shown that drifters sample randomly eddy structures *Chaigneau and Pizarro* [2005].)

(Added: Test results show that the TOEddies algorithm detects significantly fewer structures when applied to ADT maps than SLA maps. Consequently, the total area occupied by the eddies identified on ADT maps is 30 to 50% less than on SLA maps. Compared to LU16, the TOEddies identification of anticyclones on the ADT maps shows better skill, especially when eddies are identified by the maximum velocity contour. Conversely, cyclones are better identified from SLA maps. However, the fact that the number of eddies detected in ADT maps is significantly lower than that in SLA maps convinced us to use the former. We also noted that detection efficiency increases significantly when eddies are defined by their actual contours instead of assuming circular eddies with assigned equivalent radii.)

(Deleted: ~~To ensure that the comparison of TOEddies and META17 in skill against LU16 loopers is as robust as possible in terms of measurement as possible, TOEddies_rad statistics was used instead of TOEddies. Indeed, the TOEddies_rad and META17 skills are obtained by considering equivalent eddy radii instead of eddy contours. Note here that the statistics for TOEddies and TOEddies_rad are very similar, only the skill decreases slightly. TOEddies_rad is 10% more efficient and its error in eddy detection is 3 times lower than META17 in terms of eddy collocation with LU16. The ability of TOEddies_rad and META17 to encompass LU16 eddy centers as a function of eddy size is shown in Figure 8. The percentage of matches with LU16 increases while the percentage for matching errors decreases for both atlases as the LU16 vortex size increases. Both datasets are more~~

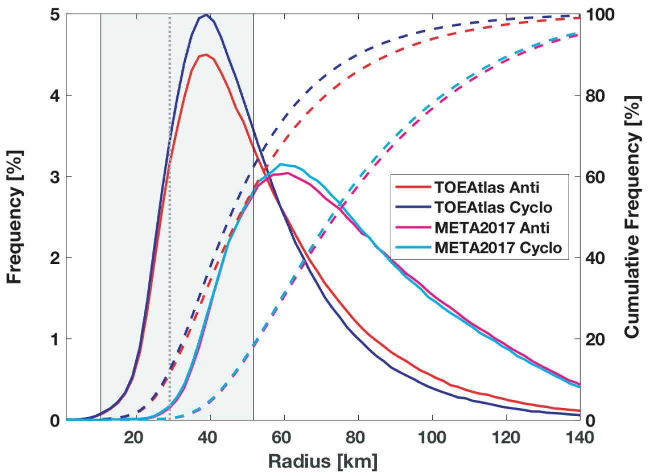

Figure 7. Histograms (solid lines) and cumulative frequency (dashed lines) of the eddy R_{max} for TOEddies (red and blue lines) and META2017 (pink and light blue lines) computed over 2-km intervals. The vertical dotted line is the mean first baroclinic Rossby radius (L_R) of deformation in the area and the grey dashed area limits the 10 and 90 percentiles. The baroclinic Rossby radius of deformation is computed by applying the *Chelton et al.* [1998] method on the World Ocean Database [*Boyer et al.*, 2013] averaged over seven years (i.e. 2005 to 2012).

~~effective in detecting small cyclones than small anticyclones and large anticyclones than large cyclones.~~)

(Deleted: ~~It can be expected that there will be a minimum size of the eddies detected from satellite altimetry maps. The ability of the two atlases, TOEddies and META17, to match the LU16 eddies as function of LU16 size is presented in Figure 8. It shows that for a radius of 25 km (which represents the average radius of the LU16 loopers, Figure 5 and the average size of the altimetry maps grid) more than 65% of the eddies are identified by TOEddies while they represent only 48% (52%) for anticyclones (cyclones) in META17. The 90% matching limit is reached, for TOEddies, for eddies with radii between 45 and 55 km, while it is 85-95 km (75-85 km) for anticyclones (cyclones) in META17. In terms of detection errors (mismatching), they are less than 1% for anticyclones (cyclones) over 15 km (10 km) in the case of TOEddies, whereas, for META17, they become as small only for anticyclones (cyclones) larger than 30 km (70 km).~~)

(Added: The comparison of TOEddies with META2017 shows that the former has better skill in both stages, eddy detection and eddy tracking. TOEddies detects more ed-

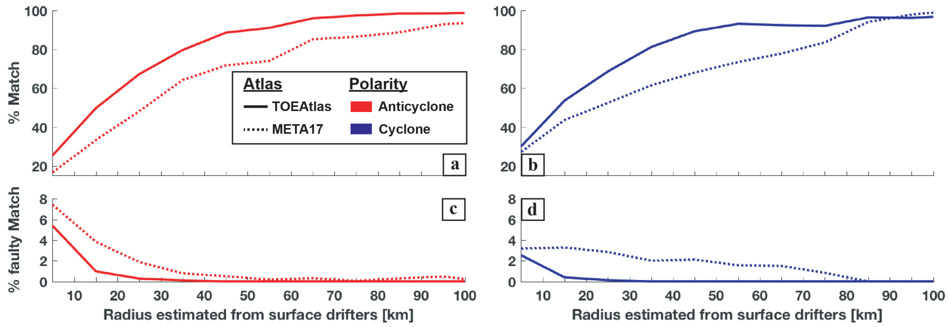

Figure 8. Percentage of matching of LU16 eddies with TOEddies (solid lines) and META2017 (dashed lines) eddies as a function of LU16 eddy size. Values are expressed as a percentage of LU16 eddies collocated at 10 km intervals. We consider that eddies match if their polarity in LU16 and in the atlases based on altimetry is the same. When the polarities of the collocalised eddies differ, this is counted as a mismatch. Anticyclones are in red, cyclones are in blue.

dies, and their size is smaller than those detected by META2017 (Figure 7). It also shows particularly good performance in identifying large structures (with a radius greater than 40 km). Figure 8 shows that for a 25 km radius (which represents the average radius of the LU16 loopers, Figure 5, and the average grid size of the altimetry maps) more than 65% of the eddies are identified by TOEddies whereas they represent only 48% (52%) for the anticyclones (cyclones) in META2017. Finally, 50% of the TOEddies trajectories correspond to those of LU16. Therefore, the results of the validation and skill assessment of TOEddies against another eddy detection method or independent data give us confidence in our algorithm in the study area. To be noted that TOEddies eddies are close in size to the regional first baroclinic Rossby Radius of deformation (Figure 7).)

(Deleted: ~~subsectionValidation of tracking filtering~~)

(Deleted: ~~In this section the ability of the two atlases, TOEddies and META17, to track eddies is examined. This ability is measured by looking at the proportion of the collocation of the eddies of the two atlases with the LU16 loopers that participate in a trajectory that lasts more than one week. The total number of LU16 trajectories used in the comparison is 431 for anticyclones and 414 for cyclones. The comparison is presented here for the three version of our atlas where we vary either the type of contours defining the eddy area (the outer contour and the velocity maximum contour) or by applying the same method in the collocation with LU16 as that used for META17.~~)

(Deleted: ~~Eddy trajectory comparison statistics are presented in Table A.2. Here the skill is measured by the overall percentage of matching between the TOEddies or META17 and LU16 trajectories. The percentage of the trajectories tracked is computed as the percentage of LU16 eddy trajectories of each polarity associated with, for at least one day, the TOEddies or META17 eddy trajectories of the same polarity. The "trajectory network" column shows the percentage of the trajectories erroneously tracked by more than one trajectory in META17 or by a first order network for TOEddies. The columns "> 50%" and "> 90%" indicate the number of LU16 trajectories collocated with the eddies defined by the other atlas during, respectively, more than 50 and 90 % of lifetime of the LU16 eddies. The "mean tracking time" column gives the average percentage of collocation time between LU16 eddies and other atlas eddies expressed in terms of the lifetime of LU16. The error estimates correspond to the collocation of eddies of different polarities for at least one day.~~)

(Deleted: ~~The results show that TOEddies skill improves when the outer eddy contour (R_{out}) instead of the maximum velocity contour (R_{Vmax}) is used to define the eddy perimeter. However, the associated mismatches are somewhat greater. Taking into account both definitions of eddy limits, between 60% and 70% of LU16 trajectories are tracked by TOEddies and between 50 and 60% of them are tracked for more than 50% of their lifetime. The reconstruction of a higher order network is necessary for less than 10% of the trajectories successfully tracked. This could be a consequence of the LU16 filtering we carried out previous to the validation processes. In fact, the merging and splitting of eddies can cause sudden changes in the spin of the drifter and an increase in the radius of the LU16 loopers, a radius that can become larger than 300 km, the maximum limit we have set for them.~~)

(Deleted: ~~Using the radius for cross detection of the structures gives results similar to those obtained using defined eddy perimeters. Table A.2 shows that the largest difference in skill is obtained for META17. Indeed, META17 identifies between 5 and 10 % fewer trajectories than TOEddiesAtlas. Moreover, the percentages obtained for TOEddies indicate that trajectories that account for eddy merging and splitting are real and well reconstructed. On the other hand, the association of more than one META17 trajectory with a LU16 suggests that META17 sometimes loses the true track of eddies. This is clear when considering the duration of collocation with LU16 loopers. Indeed, whereas between 1/2 and 1/3 of the TOEddies network recovers almost all LU16 trajectories (i.e. > 90 %), this statistics is only 1/4 for META17. Moreover, META17 trajectories follow LU16 Loopers 10% less~~

than TOEddies. The META17 mismatch cases are also more numerous (by a factor of two) than the TOEddies cases.)

(Deleted: TABLE TRACKING SKILLS)

(Deleted: subsectionSummary on the algorithm validation and skill)

(Deleted: All datasets show both, a decrease in the error and an increase in detection efficiency for LU16 eddies with large radii. This is probably due to the limited spatial resolution of satellite altimetry and its limited ability to capture small structures citep[e.g.][]Chelton:2011. However, it should be noted here that LU16 eddy radii may provide an underestimate of the true size of structures. Indeed, drifting buoys are drawn by the movement of the upper ocean at different distances from the center of the eddy and they do not necessarily move along the outer eddy edge or along the maximum velocity contour of the eddy. At contrary, these buoys sample randomly these structures as shown by citetChaigneau:2005.)

(Deleted: The TOEddies algorithm detects significantly fewer structures when applied to ADT than SLA maps. Consequently, the total area occupied by eddies identified on ADT maps is 30 to 50% less than for SLA. Compared to LU16, TOEddies anticyclones identified from ADT maps show better skill, especially when eddies are identified by the maximum velocity contour. Conversely, cyclones are better identified from SLA maps. However, the fact that the number of eddies detected in ADT maps is significantly lower than that of SLA maps persuaded us to use the former. We also noted that the detection efficiency increases significantly when eddies are defined by their actual contours instead of assuming circular eddies with assigned equivalent radii.)

(Deleted: The comparison of our algorithm with META17, shows that TOEddies has better skill in both stages, eddy detection and eddy tracking. TOEddies detects more eddies, and their size is smaller than META17. The TOEddies eddies are comparable in size to the regional first baroclinic Rossby Radius of deformation (Figure 7). It also shows particularly good performances in the identification of large structures (with radius larger than 40 km). Finally, 50% of the TOEddies trajectories correspond to those of LU16. Therefore, the results of the validation and skill assessment of TOEddies against another eddy-detection method or independent data give us confidence in our algorithm in the study area.)

4 Results of the TOEddies method applied to Agulhas Rings

4.1 Identification of Agulhas Rings and distribution of the associated trajectories

TOEddies (Replaced: ~~identified~~ replaced with: has identified, overall,) more than 3 million eddies in the daily ADT maps in the selected Indo-Atlantic domain and for the given time period (>24 years). This corresponds to 120 (Replaced: ~~thousand~~ replaced with: 000) anticyclonic (Added: trajectory)segments (Deleted: ~~of trajectories~~)identified from the full tree of segments(Replaced: ~~by~~ replaced with: ,)using the cost function. These (Replaced: ~~numbers~~ replaced with: figures) are reduced to 2.5 million eddies and 30 (Replaced: ~~thousand~~ replaced with: 000) segments after application of the (Replaced: ~~threshold of a minimum of 4 weeks lifetime.~~ replaced with: minimum 4-week lifetime threshold.) Among these eddies and segments, the Agulhas Rings (hereafter (Replaced: ~~dubbed as~~ replaced with: referred to) AR) are defined as anticyclonic eddies initially detected in the Indian Ocean sector of the domain, and entering the Atlantic Ocean by crossing an imaginary line connecting specific topographic structures (the Protea, Simpson, Wyandot, Schmit-Ott seamounts and the Agulhas Ridge) that define the southeastern limit of the Cape Basin, southwest of Africa. This line (marked with the letter "C" in Figure 10a) extends from the southern tip of Africa (Cape Agulhas, 35°S and 20°E) to 45°S and 5°E at the southern limit of the Agulhas Ridge in the Southern Ocean. This definition of AR assumes that it is possible to track these eddies (Replaced: ~~along with~~ replaced with: and) their origin and fate in order to identify them carefully. This identification is carried out for the entire ADT time series. However, in this work, we focus only on AR properties during the period January 1, 2000 to December 31, 2016 to ensure that all AR detected during this period can be tracked back to their origins. Indeed, as we will see later in this section, AR have a particular long life span and can take years to cross the Indo-Atlantic domain.

In what follows, (Deleted: ~~in order~~)to describe eddy trajectories that include eddy merging and splitting, the concept (Deleted: ~~s~~) of (Added: “)segment network(Added: ”) (Deleted: ~~is used~~)and (Replaced: ~~"~~ replaced with: “)main trajectories(Replaced: ~~"~~ replaced with: ”) introduced in Section 2.2(Added: are used). 32 080 anticyclonic eddies that (Replaced: ~~cluster~~ replaced with: group) into 122 "main trajectories" (i.e., "order 0" trajectories) are identified as AR entering the South Atlantic from the Indian Ocean. It is then possible to recover the entire network of segments associated with these "main trajec-

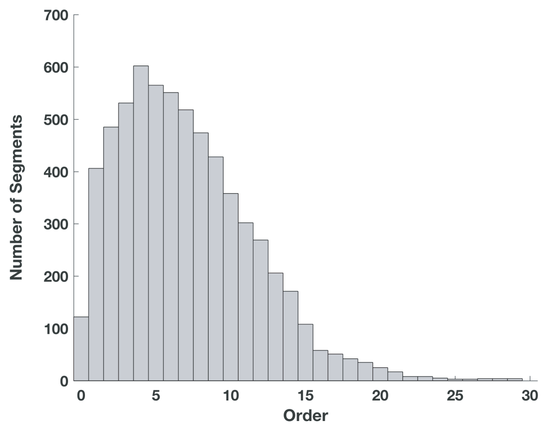

Figure 9. Number of trajectories according to their order associated with Agulhas Rings.

tories" by identifying the higher order trajectories that are linked to the main trajectories by additional merging and splitting events. The total AR network consists of secondary trajectories up to (Deleted: ~~the~~)order 29(Replaced: ~~. They combine~~ replaced with: , combining) a total of 730 481 (Added: anticyclonic)eddies and 6 363 segments.

The distribution of AR trajectories (Added: as a function of)according to their order is shown in Figure 9. The distribution is characterized by an increase in the number of segments as a function of (Deleted: ~~the~~)trajectory order, from order 0 to the peak (Replaced: ~~that corresponds~~ replaced with: corresponding) to order 4. Then(Added: ,) the number of new (Deleted: ~~,~~) higher order trajectories associated with AR reduces gradually. The (Replaced: ~~AR trajectories median order~~ replaced with: median order of the AR trajectories) is 6.

The whole set of AR trajectories (from order 0 to order 29) is presented in Figure 10a while Figure 10b shows the percentage of time during which each 2°x2° grid cell is inside an anticyclonic eddy connected to the AR trajectory network. The corresponding Figures for order 0, 1 to 4, 5 to 10, 11 to 20 and 21 to 29 (Deleted: ~~taken separately~~)are provided in Figures S1 to S5 in the Supplementary Information as well as that of the 19 302 trajectories (1 397 533 eddies) (Replaced: ~~which~~ replaced with: that) do not interact with the AR network. In the following, we will refer to (Added: the)eddies (Replaced: ~~in~~ replaced with: of) the AR network as (Added: the)AR Eddy Network (AREN)(Added: ,) which cluster(Added: s the main) AR (Deleted: ~~main~~)trajectories (i.e., order 0) and all

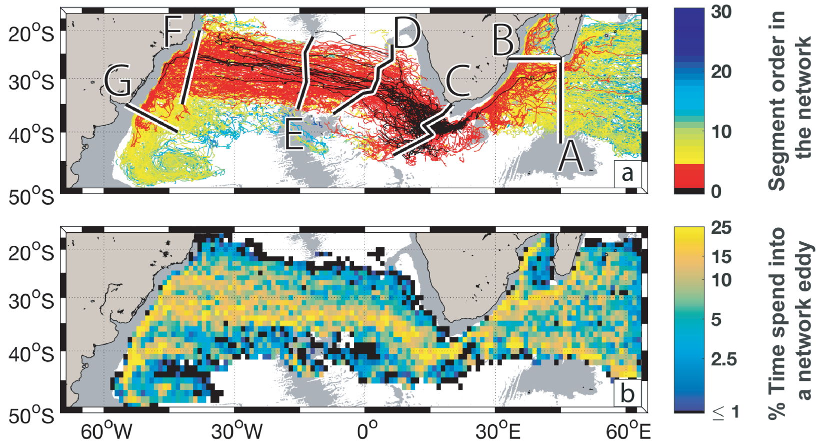

Figure 10. a) Whole set of Agulhas Ring Eddy Network (AREN) trajectories (from order 0 to maximum order 27). The color of the trajectories is related to their order. The black color is for order 0, which we defined as the main trajectories for the Agulhas Rings. 7 sections [A-G] were used to derive the AR properties across the basins. b) percentage of time each 2°x2° grid cell is within an AREN trajectory. The gray shading in each figure represents water depths less than 3500 m in the ETOPO2 data set [*Smith and Sandwell*, 1997].

the additional eddies associated (Replaced: ~~to~~ replaced with: with) them via eddy merging and splitting (Replaced: ~~up to~~ replaced with: until) the maximum order found (29).

Figure 10a shows how TOEddies provides a very different overview of the origins, pathways and fate of AR. Indeed, although the (Replaced: ~~"main"~~ replaced with: “main”) AR trajectories (in black in Figure 10a and in the Supplementary Information Figure S1) are relatively similar to the results of (Added: the)published studies [e.g., *Dencausse et al.*, 2010a; *Chelton et al.*, 2011; *Souza et al.*, 2011b], most of them are lost in the Cape Basin or associated with (Replaced: ~~some other higher-order trajectory~~ replaced with: other higher order trajectories). However, those crossing the South Atlantic basin may be directly related to AR and their region of formation, whereas in previous studies [e.g., *Byrne et al.*, 1995; *Arhan et al.*, 1999; *Souza et al.*, 2011a], this connection could not be made via an objective tracking algorithm because the first detections were (Deleted: ~~mostly~~)found (Added: mostly)in the Cape Basin, far downstream (Replaced: ~~of~~ replaced with: from) the Agulhas Retroflection. This is due to the strength of the TOEddies algorithm, which allows eddies to merge and split and to soundly connect a more complex eddy structure into a "main" trajectory instead of (Replaced: ~~only dealing~~ replaced with: dealing only) with single and well(Replaced: ~~-~~ replaced with: -)separated eddies. In addition, the complete set of AREN trajectories (Figure 10a) shows a much richer diversity in terms of origins and fate of AR, and this for AREN (Added: trajectories of)order 4 or even less (red trajectories in the Figure). The resulting AREN trajectories suggest that the eddies contributing to the formation of AR may (Replaced: ~~come~~ replaced with: originate) from the southwest(Replaced: ~~T~~ replaced with: ern t)ropical Indian Ocean, further upstream than the Agulhas Retroflection. Figure 10a shows that (Replaced: ~~an~~ replaced with: one) AR main trajectory connects directly to the area south of Madagascar. Moreover, AREN trajectories reach (Replaced: ~~far downstream regions~~ replaced with: regions further downstream) than the Cape Basin or the Mid-Atlantic Ridge in the South Atlantic. Indeed, (Replaced: ~~order 1-4 AREN trajectories~~ replaced with: AREN trajectories of orders 1-4) reach the southern end of the South Brazil Current. In particular two (Added: AREN trajectories of)order 0 AREN veer south along the South American slope. Furthermore, (Replaced: ~~higher order AREN penetrate into~~ replaced with: AREN trajectories of higher order penetrate) the Zapiola gyre. The AR trajectories estimated by TOEddies show a clear eddy pathway linking the western boundaries currents of the Indian and Atlantic oceans.

The main routes (Added: under)taken by AREN (Added: trajectories)are clearly shown in Figure 10b. Three main routes associate Indian Ocean anticyclones to AR: one follows the western boundary slope in the Mozambique Channel, another (Replaced: ~~that~~ replaced with: the slope) at the southeastern tip of Madagascar, and the third follows the Agulhas Return Current. The first two seem to merge north of the Agulhas Plateau, around 32°S and 25°E, where the Agulhas Current and the Agulhas Return Current flow in a very narrow corridor between the African slope and this plateau. West of the Agulhas Retroflection (i.e., west of line C in Figure 10a), the AREN (Added: trajectories)follow (Deleted: ~~s~~), in the Cape Basin, a broad northwesterly route toward a more zonal direction (along the 35°S parallel) once the eddies leave this basin and enter the South Atlantic. At the Mid-Atlantic Ridge, the AREN main path widens until reaching the South American slope between 25°S and 35°S. This wide route in the western part of the South Atlantic seems to consist essentially of trajectories (Replaced: ~~of~~ replaced with: from) order 0 to order 4 (Figures 10a, S2 and S3). Once they reach the South American boundary, most eddies head south with the South Brazil Current. However, some trajectories turn north along the western boundary and cross the Cruzeiro do Sul and Vitoria Trinidade seamounts.

4.2 Characteristics of the Agulhas Rings network of trajectories

(Replaced: ~~While~~ replaced with: Although) satellite altimetry gives access to (Replaced: ~~the~~ replaced with: ADT) 2D time series (Deleted: ~~of ADT~~), it does not (Deleted: ~~enable to~~)directly infer the 3D properties of eddies. However, altimetry provides sufficient information to characterize the kinematic and dynamical behavior of eddies, at least in their surface expression and as long as (Added: the)eddies are detectable from the satellite field. In particular, the TOEddies method gives access to information on (Deleted: ~~the~~)horizontal (Replaced: ~~extent of eddies~~ replaced with: eddy extent) (R_{out} and R_{Vmax}), amplitude, azimuthal velocity and propagation speed. The geographical distribution of the median of these properties is presented in Figures 11 and 12. More precise estimates of these variable(Added: s) are provided in Table 3 at fixed locations. Eddy merging and splitting lead to complex trajectories that can be independent for short periods of time. This highly complicates the description of eddies and their fate in terms of classical eddy trajectories. Indeed, an AR can be associated with many different trajectories because, during its lifetime, it splits in small (Deleted: ~~er~~) eddies and eventually merges with other eddies (which can be either AR or anticyclones of different origins). Therefore, we (Deleted: ~~have~~)decided to describe the fate of AR by counting the AREN (Added: trajectories)only when they cross particular sections (lines [A-G] in Figure 10a). In Table 3 the characteristics of the AREN (Added: trajectories)across the basin are summarized (in terms of the median and standard deviation of various properties calculated for the geographical lines A to G in Figure 10a). The contributions of the five groups of different AREN trajectory orders (0, 1-4, 5-11, 12-20, and 21-29) to the total number of AREN (Added: trajectories)crossing the control sections are presented as a percentage in Table 4.

The number of segments entering the Cape Basin since 2000 is 119. This number of segments varies across the domain due to the (Replaced: ~~many~~ replaced with: numerous) eddy-eddy interactions and (Replaced: ~~eddy vanishing from the~~ replaced with: the disappearance of eddies from) altimetry maps. The AREN median radii, R_{out} and R_{Vmax}, are relatively constant (Replaced: ~~across~~ replaced with: throughout) the domain (see Table 3 and Figure 11a). The median (± one standard deviation) R_{out} and R_{Vmax} are 79 km (± 38 km) and 59 km (± 29 km), respectively. The estimate of R_{Vmax} in the Cape Basin, where most AR are documented in the literature, (Replaced: ~~varies between~~ replaced with: ranges from) 58 (Replaced: ~~and~~ replaced with: to) 65 km which are values close to the

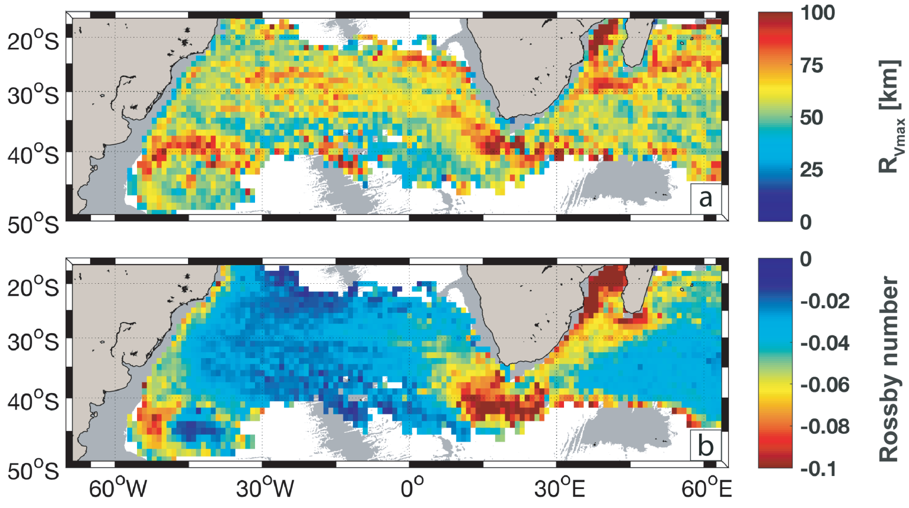

Figure 11. a) Median of Rossby number (Ro) and of the b) Equivalent radius of the characteristic contour (R_{Vmax}) of the Agulhas Ring Eddies Network. These properties are computed on a 2°x2° grid. The gray shading in each figure represents water depth shallower than 3500 m in the ETOPO2 data set [*Smith and Sandwell*, 1997].

lower limit of the 65-100 km range derived from in(Replaced: ~~-~~ replaced with:)situ observations in the Cape Basin by *Garzoli et al.* [1999] and *Arhan et al.* [1999]. The median amplitude and the azimuthal speed of the AREN are maximum (21 cm and 47 cm/s respectively) when (Replaced: ~~they enter~~ replaced with: entering) the Cape Basin. Since R_{Vmax} does not var(Replaced: ~~ies~~ replaced with: y) significantly across the entire domain (Figure 11a), the median of the eddy vortex Rossby Radius, Ro, (Figure 11b) provides an indirect measure of the changes in the eddy azimuthal velocity. This velocity is (Replaced: ~~maximum~~ replaced with: highest) in the Agulhas Current System and in the southern(Replaced: ~~-~~ replaced with:)half of the Cape Basin and from there it decreases rapidly and remains constant across the South Atlantic (Replaced: ~~o~~ replaced with: O)cean. It is only when the AREN (Added: trajectories)reach the South American boundary that Ro increases again, (Replaced: ~~very~~ replaced with: most) likely due to the interactions of eddies with the South Brazil Current and local anticyclones.

In addition to the inherent properties of (Replaced: ~~AREN~~ replaced with: the AREN eddies) it is (Deleted: ~~also~~)interesting to evaluate their median propagation speed (Figure 12), as it can be used to estimate the(Added: ir) transit time (Deleted: ~~of AREN~~)

Table 3. Properties of the Agulhas Ring Eddy Network throughout the geographical domain. The values are computed at the lines [A-G] plotted in Figure 10a. For each variable, estimates of the median and standard deviation (STD) are provided.

Segment of control	Number of Segments	R_{out} [km] Median ± STD	Amplitude [m] Median ± STD	R_{Vmax} [km] Median ± STD	V_{max} [m/s] Median ± STD
A: SW Indian Ocean	191	78 ± 43	0.08 ± 0.11	60 ± 35	0.22 ± 0.16
B: Mozambique Channel	30	94 ± 38	0.13 ± 0.14	66 ± 29	0.40 ± 0.17
C: SE Cape Basin	119	81 ± 38	0.21 ± 0.21	65 ± 30	0.47 ± 0.23
D: Walvis Ridge	160	91 ± 39	0.08 ± 0.09	58 ± 22	0.18 ± 0.11
E: Mid-Atlantic Ridge	167	87 ± 42	0.05 ± 0.06	64 ± 27	0.12 ± 0.07
F: S. American Slope	217	74 ± 33	0.04 ± 0.03	57 ± 27	0.12 ± 0.04
G: S. Brazil Current	71	88 ± 41	0.13 ± 0.11	74 ± 37	0.29 ± 0.12

Table 4. Distribution of the orders of the Agulhas Ring Eddy Network expressed as percentage when they cross the lines [A-G] plotted in Figure 10a.

Segments of control	Order 0 [%]	Orders 1 to 4 [%]	Orders 5 to 10 [%]	Orders 11 to 20 [%]	Orders 21 to 29 [%]
A: South-west Indian Ocean	1	9	66	22	2
B: Mozambique Channel	0	27	60	13	0
C: Southeastern Cape Basin	100	0	0	0	0
D: Walvis Ridge	12	80	8	0	0
E: Mid-Atlantic Ridge	7	75	16	2	0
F: South American Slope	2	44	52	7	0
G: Southern Brazil Current	0	13	80	7	0

through the different zones. The regions where AREN (Added: eddies)move faster correspond to the western boundary currents (WBCs) of the Indian Ocean but also of the South Atlantic (reaching speeds higher than 0.1 m/s). The AREN propagation speed remains high in the Cape Basin (although it is higher in the Southern than in the Northern Cape Basin) and in the South Atlantic, especially for the northern sector of the route, west of the Mid-Atlantic Ridge. The (Added: AREN)direction of propagation (Deleted: ~~of the AREN~~)(Figure 12b) clearly shows different regimes of fast southwestward flow in the WBCs, northwestward flow in the Cape Basin and westward flow in the South Atlantic. It also shows that the AREN path along the Agulhas Return Current involves eddies moving eastward. These eddies are most likely related to AR as a product of AR splitting in the Agulhas Retroflection area (Replaced: ~~that~~ replaced with: which) are successively advected eastward in (Deleted: ~~to~~) the intense Agulhas Return Current.

To better characterize the kinematics and dynamics of the AREN(Added: eddies), their median propagation velocity can be compared with the mean surface geostrophic velocity estimated from AVISO satellite altimetry (Figure 13). The AREN and AVISO estimates of velocity intensities compare relatively well in terms of (Replaced: ~~direction of propagation~~ replaced with: propagation direction) with the mean surface velocity in the

WBCs and the Agulhas Return Current with, in general and, as expected, (Added: the)AREN propagation speed being an order of magnitude less than the surface geostrophic velocity. Here, the eddies are advected with the mean current. However, differences between (Deleted: ~~the mean~~)AVISO and AREN (Added: mean)velocities occur in the northern subtropical South Atlantic where eddies appear to move westward at a higher velocity (about 6 cm/s) than the mean surface geostrophic velocity (about 2 to 4 cm/s), and in the southern subtropical Atlantic (south of 30°S) where they move westward against the mean surface current (which flows eastward as expected for the (Replaced: ~~polarward~~ replaced with: poleward) branch of the South Atlantic gyre: see Figure 12, Figure 13, and Figure 1b). The ratio of the AREN translation speed and the mean geostrophic current are computed in each 2°x2° grid cell (Figure S7 in the Supplementary Information). It shows that AREN move faster than the mean surface gesotrophic current in 60% of these cells.

McDonagh et al. [1999] studied the (Deleted: ~~contribution~~)mechanisms responsible for the translation of Agulhas Rings in the Cape Basin. They showed from two specific AR that the self(Replaced: ~~-~~ replaced with: -)advection mechanism [*Rhines*, 1975; *Cushman-Roisin et al.*, 1990] is not sufficient and conclude that the main factor appears to be the advection by the main flow. These results are (Replaced: ~~in good agreement~~ replaced with: consistent) with our findings that high AREN translation values are found where (Deleted: ~~the~~)geostrophic surface velocities are also important. This is verified in the WBCs and in the Cape Basin. However, in the South Atlantic, AREN (Added: eddies)move faster(Added: ,) if not against the surface geostrophic flow. Here, most likely, the main mechanism of translation is the self(Replaced: ~~-~~ replaced with: -)advection of eddie(Added: s) (Deleted: ~~and the eddy-eddy interactions~~).

4.3 Agulhas Rings origins, disappearance, splitting and merging

To better describe the AREN, we discuss here the statistics in the regions where they are initially identified, where they disappear as well as the distribution of eddy merging and splitting events. The description of AR as anticyclonic eddies participating in the AREN may not be appropriate (Replaced: ~~as~~ replaced with: because) they are associated with a large number of eddy merging and splitting (Replaced: ~~occurrences~~ replaced with: events) (i.e. high order (Deleted: ~~s~~) trajectories). For this reason, we (Replaced: ~~have placed~~ replaced with: put) a particular emphasis on estimates of AREN trajectories up to order 4(Added: ,) which correspond to the peak of the number of trajectories as (Added:

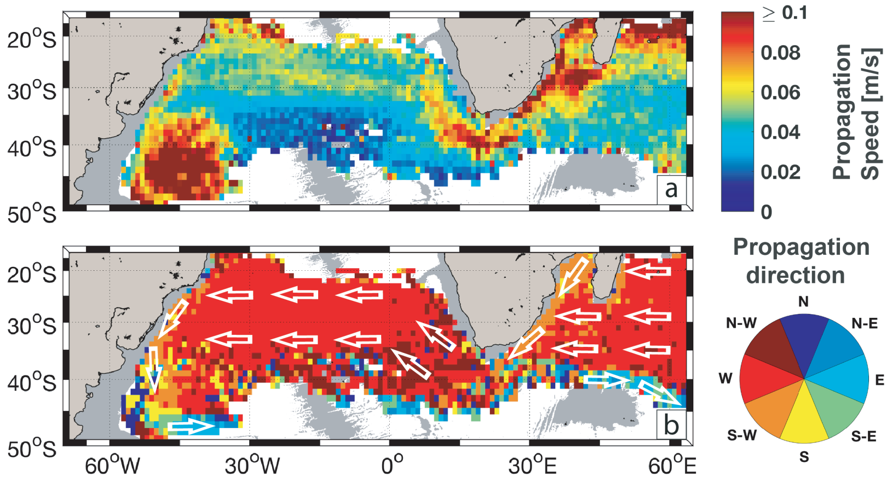

Figure 12. a) Median of the propagation velocity of the Agulhas Ring Eddy Network (in m/s) and b) associated main propagation direction. These properties are calculated on a 2°x2° grid and the propagation direction is computed from the eddy positions one week apart. Schematic white arrows have been added in the bottom panel to highlight the main propagation direction. The gray shading in each figure represents water depth shallower than 3500 m in the ETOPO2 data set [*Smith and Sandwell*, 1997].

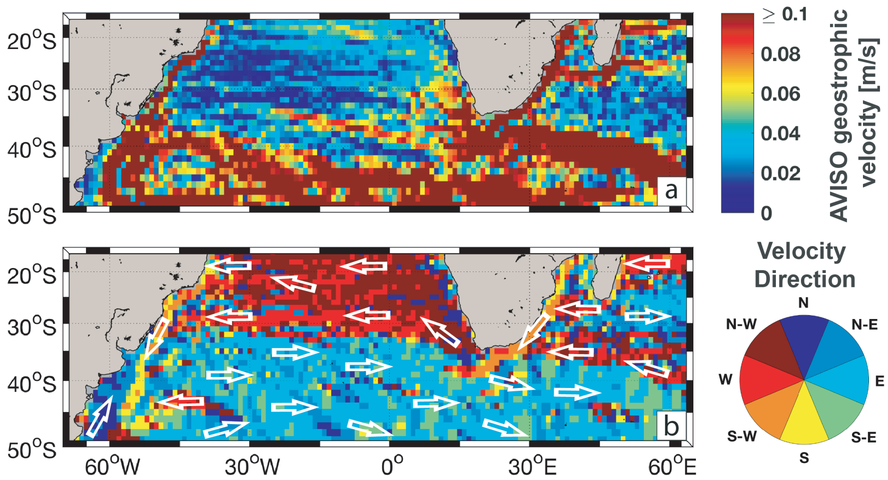

Figure 13. a) Mean surface geostrophic velocity estimated from AVISO satellite altimetry (in m/s) and b) associated main direction. These properties are computed on a 2°x2° grid. Schematic white arrows have been added in the bottom panel to highlight the main velocity direction. The gray shading in each figure represents water depth less than 3500 m in the ETOPO2 data set [*Smith and Sandwell*, 1997].

a)function of the trajectory order (Figure 9). In the following, we will (Replaced: ~~refer to~~ replaced with: call) this subgroup of AREN(Replaced: ~~as~~ replaced with: ,) AREN4.

The distribution of eddy formation, disappearance, and merging and splitting within (Deleted: ~~the~~)AREN4 (Replaced: ~~are~~ replaced with: is) presented in Figure 14 and (Replaced: ~~those~~ replaced with: that) of the total AREN in Figure 15. To better assess the regionalization of these processes, only the 2°x2° cells showing more than 5 (10) or 10 (10) first/last detections (merging/splitting) events for (Deleted: ~~, respectively,~~) AREN4 and AREN(Added: , respectively,) are presented. The difference in threshold used for the two different type(Added: s) of events is explained by the fact that TOEddies records ~(Replaced: ~~2 times more~~ replaced with: twice as many) trajectory interactions (Replaced: ~~than~~ replaced with: as) eddy formation or disappearance events. 119 AREN cross, flowing west, line C in Figure 10 (Table 3). This line defines the AR trajectories(Added: ,) which explains why only 0-order eddies enter the Cape Basin (Table 4). Most AR are initially identified at the Agulhas Retroflection as shown by the large red patches near the Cape Basin in Figure 14a and (Deleted: ~~by~~)the starting points of the black and red trajectories in Figure 10a. This region extends over a large area, between the Agulhas Bank, the Agulhas Plateau and the Agulhas Ridge, and agrees with the entire Agulhas Retroflection position (Deleted: ~~range~~), from 8°E to 25°E-28°E [e.g., *Lutjeharms and Ballegooyen*, 1988; *Dencausse et al.*, 2010b].

In addition to this traditional view of AR shedding from the Agulhas Current at the Agulhas Retroflection, our method identifies anticyclonic eddies formed at the southern (Replaced: ~~limit~~ replaced with: edge) of the Agulhas Return Current as previously observed by *Lutjeharms and Ballegooyen* [1988] and *Boebel et al.* [2003a]. (Deleted: ~~113 of the 888 east of 30°E.~~)Indeed, some eddies can merge with or split from a newly shed AR which (Replaced: ~~explains~~ replaced with: is) why we classify them as AREN. (Replaced: ~~Numerous~~ replaced with: Many) new AREN4 are located (Replaced: ~~close~~ replaced with: near) to the African continent in the northeastern part of the Cape Basin. Other locations of AREN4 origins appear near the Walvis Ridge (Replaced: ~~as well as~~ replaced with: and) further west the South Atlantic. These areas of eddy formation may be related (Replaced: ~~with~~ replaced with: to) splitting (Replaced: ~~occurrences from~~ replaced with: of) AREN4 (Replaced: ~~trajectories~~ replaced with: eddies) or (Added: to)the merging of eddies of distinct origins with AREN4 trajectories.

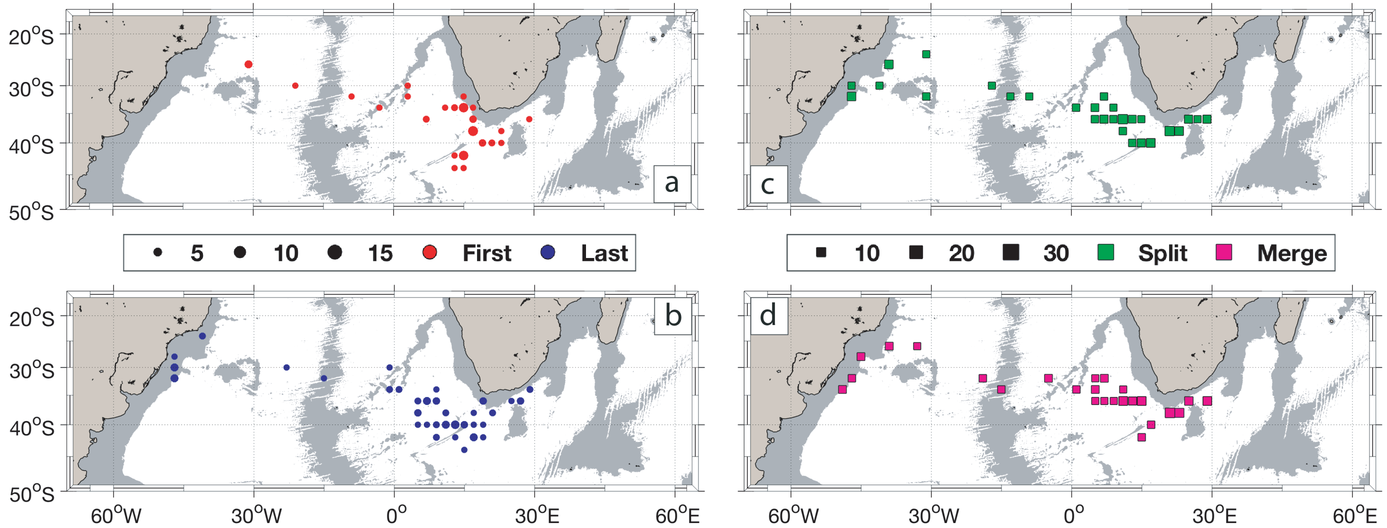

Figure 14. 2°x2° gridded positions and number of first detections (a), last detections (b) , merging events (c) and splitting events (d) of the AREN4 (i.e. AREN with orders less than 4). Each dot size represents the number of events for each grid cell associated with more than 10 occurrences. The gray shading in each figure represents water depth shallower than 3500 m in the ETOPO2 data set [*Smith and Sandwell*, 1997].

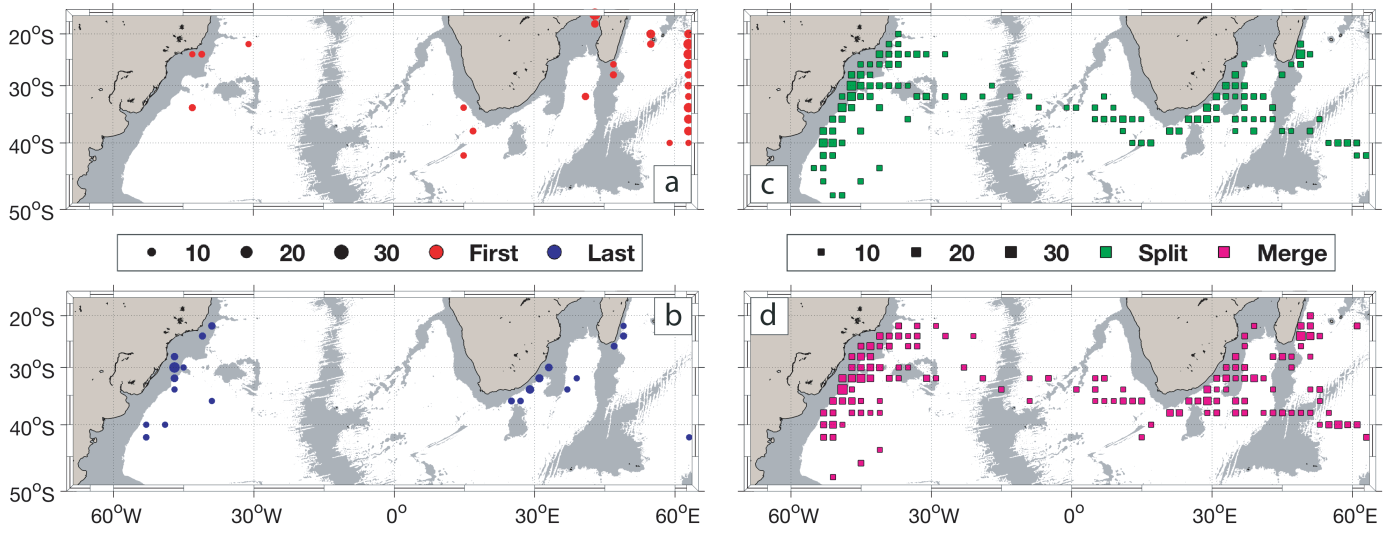

Figure 15. 2°x2° gridded positions and number of first detections (a), last detections (b) , merging events (c) and splitting events (d) of the AREN. Each dot size represents the number of events for each grid cell associated with more than 10 occurrences. The gray shading in each figure represents water depth shallower than 3500 m in the ETOPO2 data set [*Smith and Sandwell*, 1997].

(Replaced: ~~Moreover, t~~ replaced with: Moreover,113 of the 888 anticyclonic eddies that start an AREN4 trajectory are east of 30°E. T)aking into account the AREN as a whole (Figure 15), the results suggest that a relatively small number of AREN4 originate as far north as the Mozambique Channel or east of the Madagascar Ridge while (Replaced: ~~numerous trajectories of higher order AREN are as shown in~~ replaced with: many higher-order AREN trajectories are as it appears from) Table 4. Only one third of the AREN (Added: trajectories)formed in the Mozambique Channel are reconstructed (Deleted: ~~by~~)taking into account trajectories of order 4 or less, whereas 90% of the trajectories originating in the Southwest Indian Ocean are obtained (Added: by)taking into account trajectories at orders (Replaced: ~~higher~~ replaced with: greater) than 4. Figure 10b, which highlights the area where many AREN (Added: eddies)are present over the period of interest, shows a clear (Replaced: ~~connection~~ replaced with: link) between these northeast (Deleted: ~~ern~~) formation regions and the Agulhas Retroflection. This pattern is very similar to the many large eddies detected from surface drifters documented by *Zheng et al.* [2015] .

The existence of these anticyclones and their possible role in the destabilization of the Agulhas Current, leading to meanders, have (Deleted: ~~been~~)already (Added: been)documented [e.g., *Schouten et al.*, 2002; *Penven et al.*, 2006; *Biastoch et al.*, 2008a,b; *Halo et al.*, 2014; *Elipot and Beal*, 2015]. *Schouten et al.* [2002] (Replaced: ~~similarly~~ replaced with: also) found that some of these eddies do not create meanders and are advected downstream to the Retroflection. Detections of these eddies could be associated with an artificial interruption of the Agulhas Current due to the interpolation used to estimate the gridded altimetry field from the altimeters along-track data. However, the amplitude of these eddies is greater than 10 cm near the Agulhas Current. Therefore, they appear to be well-defined structures and not an artifact of data interpolation. A composite view of the (Deleted: ~~trajectory at~~)0-order (Added: trajectory)that originates from the southern tip of Madagascar is shown in Figure 16a. This eddy (Replaced: ~~is formed close~~ replaced with: forms) near Madagascar and remains very coherent until it reaches the Cape Basin. Furthermore, (Replaced: ~~these~~ replaced with: this tupe of) eddies (Replaced: ~~are~~ replaced with: is) also well captured by looping drifters [*Zheng et al.*, 2015; *Lumpkin*, 2016] and the in-situ data recorded by current meter moorings [*Donohue et al.*, 2000]. Many new detections of AREN (Added: eddies are)also occur(Added: ring) in the open Indian ocean(Added: , which)correspond(Replaced: ~~ing~~ replaced with: s) to the

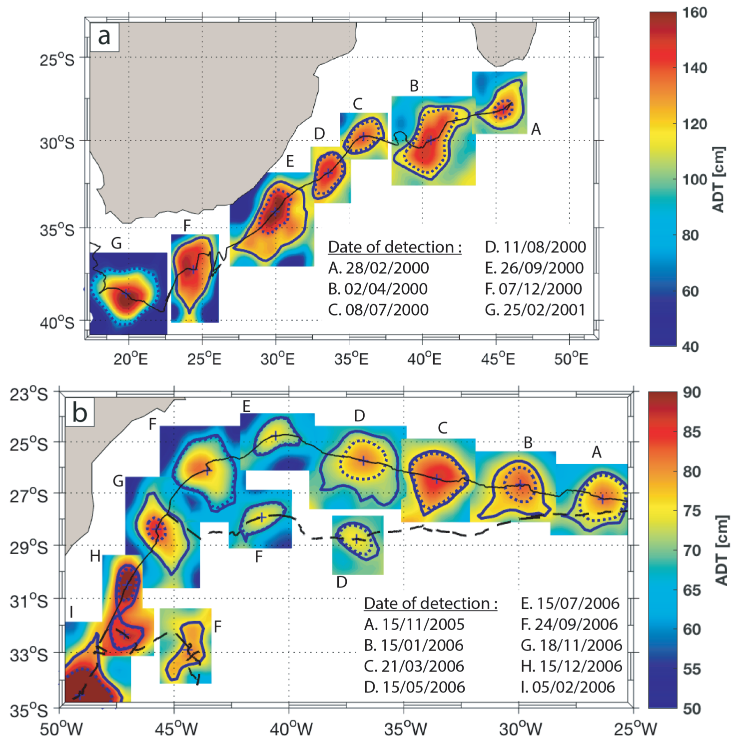

Figure 16. Composite figure of the order-0 AREN starting the most to the east (a) and ending the most to the west (b). Snapshots on selected dates are given, with in blue the eddy centroid (cross symbol), the ADT contour associated with the maximum speed (dotted) and the outermost ADT (solid line) contours. The trajectory of panel b interacts with two order-1 trajectories whose paths are drawn in dashed lines.

eastern part of our (Replaced: ~~study domain~~ replaced with: domain of study). In particular, Reunion Island, southeast of Madagascar, seems to be an active region for (Added: the identification of)new AREN (Replaced: ~~identification~~ replaced with: eddies). In summary, our results suggest that AR can form upstream of the Agulhas Retroflection, move relatively rapidly southward with the Agulhas Current (Figure 10d) until they are blocked between the Agulhas Current and its Return Current in the Retroflection area where they may merge with another eddy or be shed.

While AR origins have (Deleted: ~~been~~)often (Added: been)discussed in the literature, (Replaced: ~~albeit~~ replaced with: although) not in the more complex context of (Added: the)AREN, their disappearance has not (Added: yet)been examined (Replaced: ~~extensively yet~~ replaced with: thoroughly). The TOEddies method and the AREN approach make it possible to quantitatively infer the vanishing of AR from satellite altimetry maps. Figure 14b documents a very well(Replaced: ~~–~~ replaced with: -)structured pattern for the main regions where TOEddies lo (Deleted: ~~o~~)se the AREN4 ADT signature. This occurs mainly in the Cape Basin, not far from the (Replaced: ~~major~~ replaced with: main) source regions (Replaced: ~~for~~ replaced with: of) AREN4. (Replaced: ~~It~~ replaced with: This) suggests that most (Deleted: ~~of the~~)AREN4 (Replaced: ~~track~~ replaced with: trajectories) are lost within the Cape Basin, relatively soon after entering (Replaced: ~~this~~ replaced with: the) region. The general pattern of disappearance of AREN4 is not evenly distributed: Most eddies disappear in the southern half of the basin as well as (Replaced: ~~close to~~ replaced with: near) the Walvis Ridge. Other regions where AREN4 vanish from ADT maps are found (Replaced: ~~N~~ replaced with: n)orth of the Agulhas Plateau, (Replaced: ~~S~~ replaced with: s)outh of Africa, and near the South American slope. There is no appearance or disappearance of AR, within AREN4, in the open ocean in the South Atlantic except occasionally.

According to the TOEddies method, (Added: there are)more merging and splitting events (Deleted: ~~occur~~)than appearance and disappearance. The recurrence of such eddy-eddy interactions in the Retroflection area and in the Cape Basin has been demonstrated by various authors from in(Replaced: ~~-~~ replaced with:)situ (Deleted: ~~data~~)and remote sensing (Added: data)[*Byrne et al.*, 1995; *Arhan et al.*, 1999; *Boebel et al.*, 2003b; *Dencausse et al.*, 2010a; *Baker-Yeboah et al.*, 2010]. Our study shows that these regions correspond (Deleted: ~~indeed~~)to area(Added: s) where these process(Added: es) are particularly active (Figures 14b and c). (Replaced: ~~The t~~ replaced with: T)opographic features are also regions where (Replaced: ~~numerous~~ replaced with: many) merging and spli(Added: t)ting events (Replaced: ~~take place~~ replaced with: occur).

To complete the description of AR behavior in the South Atlantic, (Replaced: ~~in the following sections, we discuss more in depth~~ replaced with: we discuss in the following sections) the AREN regional behavior and statistics(Added: in more detail).

4.4 Agulhas Rings in the Cape Basin

Taking into account our definition of AR (anticyclones leaving the Indian Ocean and entering the Cape Basin, Figure 10a) we have identified 119 AREN4 (see Table 3). This is equivalent to a rate of 7 AR entering the Cape Basin per year. This represents a higher ratio than previous estimates (Replaced: ~~which were suggesting typically one event~~ replaced with: that typically suggested) every two to three months [e.g., *Gordon and Haxby*, 1990; *Goni et al.*, 1997; *Schouten et al.*, 2002]. However, some authors [*Schouten et al.*, 2000; *Baker-Yeboah et al.*, 2010; *Dencausse et al.*, 2010a] suggested that AR often split shortly after their shedding from the Agulhas Retroflection(Replaced: ~~and this~~ replaced with: ,) before entering the Cape Basin. This may explain why our estimate is higher than those provided in previous studies that did (Replaced: ~~not consider~~ replaced with: account for) splitting events. Indeed, eddy splitting and merging are particularly abundant near the Retroflection area (Figure 14c).

Looking separately at newly formed AR and those resulting from a splitting, we find a mean value of 4.3/year for newly formed AR entering the Cape Basin (i.e. a total of 73) while 2.8/year (Deleted: ~~of them~~)result from a splitting. Thus, about two third(Added: s) of the AR entering the Cape Basin are newly formed and the (Replaced: ~~rest of them~~ replaced with: remainder) result from a splitting. These results are very similar to those of *Dencausse et al.* [2010a] (Replaced: ~~albeit~~ replaced with: although) their estimate is twice as high. To conclude, on average, every 2.8 months(Added: ,) a newly formed AR enters the Cape Basin. This rate is very similar to those found in the literature in terms of AR shedding [e.g., *Gordon and Haxby*, 1990; *Goni et al.*, 1997; *Schouten et al.*, 2002].

At the Agulhas Retroflection and in the southern Cape Basin, the AREN trajectories are (Added: essentially)made (Deleted: ~~essentially~~)by AREN4 (i.e., rows C and D in Table 4 and Figures S1 to S5 in the Suplementary(Added: information)). Here, AREN are characterized by large Ro (Figure 11a) in the area where they are (Added: mainly)spawned (Deleted: ~~primarly~~)(Figure 14a and line C in Table 3). A sudden transition in Ro appears (Replaced: ~~as~~ replaced with: when) AR enter the Cape Basin (Figure 10b and 11a). This transition is due to a decrease in AR surface V_{max} and amplitude (and thus surface vorticity), whereas the radii remain relatively constant (Table 3). A decrease in vorticity in the Cape Basin has already been observed although not quantitatively documented [e.g., *van Sebille et al.*, 2010].

Eddies in the Cape Basin have a particularly complex behavior that has (Deleted: ~~already~~)been suggested by previous studies [e.g., *Arhan et al.*, 1999; *Schouten et al.*, 2000; *Boebel et al.*, 2003b; *Dencausse et al.*, 2010a]. Here(Added: ,) we can try to characterize (Replaced: ~~such~~ replaced with: this type of) behavior more extensively. As already mentioned, TOEddies takes into account numerous AR separations and coalescences throughout the Cape Basin (Figure 14c and d). Although Figure 14b shows a main (Replaced: ~~AR northwesterly path~~ replaced with: path of AR to the northwest) suggesting straight trajectories, their individual behavior is truly complex due to eddy-eddy interactions, and induces relatively long residence times. The real impossibility of associating a trajectory with a single eddy but (Replaced: ~~instead~~ replaced with: rather) the need to consider the full set of AREN trajectories complicates the definition of a mean residence time associated with AR for each specific region of the domain considered. We propose here to overcome this difficulty by considering (Replaced: ~~the whole set of~~ replaced with: all the) AREN trajectories reconstructed from (Replaced: ~~every~~ replaced with: each) segment crossing each line in Figure 10a. In this way(Added: ,) we can estimate the residence time of the AREN (Added: eddies)in the Cape Basin by considering the segments that cross the Walvis Ridge (i.e. Line D in Figure 10a) and that are associated (backward in time) with segments that cross the southeast limit of the Cape Basin (i.e. Line C in the Figure 10a). We limit the reconstruction of the network to(Added: trajectories of) order 15 (Deleted: ~~trajectories~~).

100 of the 119 AREN4 trajectories crossing line C are associated with a median order (Replaced: ~~equal to~~ replaced with: of) 2 (i.e. 2 eddy-eddy interactions that include eddy splitting and merging). (Replaced: ~~Considering~~ replaced with: Based on) these trajectories, we find that the mean residence time of AR i(Replaced: ~~n~~ replaced with: s) the Cape Basin in about one year (median of 1.0 ± 0.5 years)(Added: ,) which corresponds to the estimate of *Schouten et al.* [2000]. During their journey in the Cape Basin, AR undergo (Deleted: ~~to~~)important changes affecting their surface signature, as shown in Figures 11, 12 and Table 3 in terms of several dynamical and kinematic properties. In particular, although their sizes remain relatively stable, their initial surface signatures in amplitude, Ro and V_{max} (Replaced: ~~drop~~ replaced with: decrease) by ~50% (Replaced: ~~i~~ replaced with: o)n average.

While 119 AREN4 enter the Cape Basin, 160 cross the Walvis Ridge and enter the South Atlantic (Table 4). Again, because TOEddies does not associate a trajectory with a single eddy, these two values cannot be linked directly. Indeed, the number of eddy splitting and merging (Added: events)in the Cape Basin is very high (Figure 14c) as is (Replaced: ~~that~~ replaced with: the number) of eddy disappearance(Added: s). In particular, Figure 14b shows that many of the initial 119 AR are lost on satellite altimetry maps in the southern Cape Basin.

4.5 Agulhas Rings across the South Atlantic

The fate of the 119 AREN4 that cross the Walvis Ridge and enter the South Atlantic Basin appears more linear and less turbulent than in the Cape Basin. They flow in a very zonal direction (centered around 35 ° S and about 5° wide). Here, their disappearance from the altimetry maps is almost nil (Figure 14b for AREN4 and Figure 15b for the whole AREN). The number of merging and splitting events is also (Replaced: ~~drastically decreased~~ replaced with: significantly reduced). The main area where eddy-eddy interactions become important again corresponds to the Rio Grand Rise in the western part of the South Atlantic while the Mid-Atlantic ridge is not associated with such events but has an impact on the (Added: AREN)zonal route (Deleted: ~~of AREN~~)by increasing its width (which becomes 10° wide).

A large portion of the AREN4 crossing the Walvis Ridge reaches the Mid-Atlantic Ridge (line E in Figure 10a) which represent 82% of the AREN passing this ridge. The very coherent behavior of the AREN crossing the South Atlantic is well captured by reconstructing the network and crossing times between lines E and D. On average, AREN (Added: eddies)cross the eastern South Atlantic in about 1 year (a median time of 1.0 ± 0.3 years) with a median of only 1 eddy-eddy interaction (Deleted: ~~s~~). However, (Added: the)AREN behavior changes on the other side of the Mid-Atlantic Ridge. Here, the contribution of AREN4 to AREN reaching the South American slope is only 46%. This may be the result (Deleted: ~~s~~) of the numerous eddy-eddy interactions at the Rio Grand Rise (Replaced: ~~which~~ replaced with: that) has an impact on the overall behavior of the trajectories. The western part of the South Atlantic is crossed in 1.5 year(Added: s) (a median value of 1.5 ± 0.6 years computed between lines E and F) with a median of 3 eddy-eddy interactions.

Finally, Figure 10c shows a clear decrease in the surface intensity (Ro) of AREN (Added: eddies)across the South Atlantic, associated with a 43% (Deleted: ~~surface~~)decrease in their (Added: surface)azimuthal velocity V_{max} and 60% in their amplitude, while their size remains relatively stable (from lines D to F in Table 3).

Many authors [e.g., *Gordon and Haxby*, 1990; *Byrne et al.*, 1995; *Schouten et al.*, 2000] have demonstrated the ability of AR to penetrate the South Atlantic Ocean, (Replaced: ~~alleging~~ replaced with: claiming) that they gradually dissipate and vanish in this basin. Our study suggests a different fate for these eddies (Replaced: ~~as~~ replaced with:

since) nearly half of the AREN4 reaches the South American continent. Among these 4 of such trajectories are 0-order AREN.

4.6 Agulhas Rings along the South American margin

Despite their relatively low surface signature, the few AREN (Added: eddies)that are still detectable by satellite altimetry and that reach the American slope maintain their coherence. Near the South-American coast, they propagate southward in the South Brazil Current (Figure 10) for about half of a year (0.9 ± 0.5), as (Deleted: ~~already~~)suggested by *Byrne et al.* [1995]. Along this path, AREN (Added: eddies)undergo numerous eddy-eddy interactions as indicated by the large number of merging and splitting events (Figure 15b). These interactions are characterized by a sudden increase in (Deleted: ~~the AREN~~)surface signature and propagation speed (Figures 11 and 12). Moreover, some newly formed anticyclonic eddies are identified as AREN (Replaced: ~~as~~ replaced with: when) they merge with older structures. A composite view of the trajectory at 0-order that ends (Replaced: ~~most westerly~~ replaced with: further west) is shown in Figure 16a. This AR veers south when (Replaced: ~~reaching~~ replaced with: it reaches) the South-American coast. There, another anticyclonic eddy merges with it in October 2006. Two months (Replaced: ~~after~~ replaced with: later), the (Deleted: ~~0-order~~)trajectory (Added: of order 0)merges with a newly formed anticyclone (Replaced: ~~that~~ replaced with: which) results in(Replaced: ~~to~~ replaced with: t)he formation of an intense (Added: and)large anticyclone.

At the southern (Replaced: ~~edge~~ replaced with: limit) of the Brazil Current and in the Zapiola Gyre, AREN (Added: eddies)show an intense surface signature, as high as in the Cape Basin, before their trace is gradually lost. However, assessing the effective contribution of the original AR to these long trajectories remains a challenge due to the numerous eddy(Replaced: ~~-~~ replaced with:)merging and splitting events that (Deleted: ~~have~~)occurred during their lifetime, and, in particular, along the Brazilian continental slope.

5 Summary and Conclusions

In this study, we (Replaced: ~~developed~~ replaced with: present TOEddies,) a new eddy identification and tracking algorithm(Replaced: ~~, TOEddies, which~~ replaced with: that) takes into account the detection of eddy splitting and merging events (Replaced: ~~that~~

~~was~~ replaced with: which has been) applied to (Deleted: ~~the~~)gridded multi-satellite ADT maps. (Replaced: ~~Due to~~ replaced with: Because of) the many eddy-eddy interactions and the resulting eddy subdivisions and coalescences, the concept of a trajectory associated with a single eddy becomes (Replaced: ~~meaningless~~ replaced with: less obvious than previously admited). However, to be able to track the origins, fate and changes of these eddies we(Added: have) reconstructed a network of segments and trajectories (Replaced: ~~which enable~~ replaced with: that allow us) to reconstruct the (Replaced: ~~eddies' history~~ replaced with: history of the eddies).

We (Deleted: ~~have~~)also developed a method to objectively assess the robustness and skill of TOEddies against (Replaced: ~~"~~ replaced with: “)loopers(Replaced: ~~"~~ replaced with: ”), an eddy atlas derived from the completely independent (Deleted: ~~data~~)set of drifting buoy(Replaced: ~~s~~ replaced with: data) [*Lumpkin*, 2016]. This allowed us to quantitatively compare and test TOEddies against the eddy atlas distributed by SSALTO/DUACS [*Duacs/AVISO+*, 2017]. TOEddies proved to be more robust (Deleted: ~~than the eddy atlas distributed by AVISO~~) because the eddies it detects (Replaced: ~~match~~ replaced with: correspond) better (by 10 % and with a smaller error) (Added: to)those identified from the surface drifter (Deleted: ~~s~~) data. (Deleted: ~~Moreover, the sizes obtained from TOEddies are in the range of the local first baroclinic Rossby Radius of deformation.~~)

After validation, this algorithm was applied to daily AVISO ADT maps from 1993 to mid-2017 to uncover and characterize quantitatively the dynamics of Agulhas Rings entering the South Atlantic Ocean. After the complete recovery of the trajectories, the eddy statistics from January 2000 to December 2016 were explored. To differentiate with the stricto-sensu definition of Agulhas Rings formed in the Indian Ocean and disappearing in the South Atlantic, we used the concept of trajectory network(Added: s) to define the Agulhas Rings Eddy Network (AREN).

The characteristics of the AREN, such as their surface signature and propagation speed near the Agulhas Retroflection, compare particularly well with previous estimates produced for a limited number of structures [e.g., *Gordon and Haxby*, 1990; *Garzoli et al.*, 1999; *Arhan et al.*, 1999; *Schouten et al.*, 2002; *Dencausse et al.*, 2010a]. However, our study contradicts the traditional view of large coherent Agulhas Rings shed at the Agulhas Retroflection that (Replaced: ~~propagate and rapidly dissipate~~ replaced with: are propagating and dissipating rapidly) in the South Atlantic Ocean. For example, our results suggest that Agulhas Rings, and other anticyclonic eddies connected (Deleted: ~~to them~~)via merging and splitting (Deleted: ~~occurrences~~), may originate as far upstream from the Agulhas Retroflection as in the Mozambique Channel or South of Madagascar. From there(Added: ,) they are advected southward by the Agulhas Current as distinct coherent structures without being absorbed or dissipated by the current.

Throughout their existence, Agulhas Rings interact intensely with neighboring eddies, giving rise to very complex trajectories. These interactions are particularly vigorous in the Cape Basin and influence the time these eddies spend in the region which is, on average, relatively long (about 1 year). Here, they undergo major changes in their surface properties (dynamic height, azimuthal velocity) while their lateral size remains relatively constant. These changes are likely due to local air-sea, eddy-eddy and eddy-topography interactions [*Arhan et al.*, 1999; *Dencausse et al.*, 2010a; *Arhan et al.*, 2011].

Numerous Agulhas Rings disappear from altimetry maps in the Cape Basin preventing their subsequent tracking. This may be due to (Replaced: ~~AR~~ replaced with: their) subduction in the ocean interior and not necessarily to eddy dissipation (Replaced: ~~as,~~ replaced with: because) in this region, (Replaced: ~~AR~~ replaced with: Agulhas Rings) release large amounts of heat in the atmosphere and become denser [*Arhan et al.*, 2011]. Indeed, evidence of (Replaced: ~~AR~~ replaced with: their) subduction (Replaced: ~~was~~ replaced with: has been) observed by *Arhan et al.* [1999] and *Garzoli et al.* [1999]. Based on these observations, *Herbette et al.* [2004] used an idealized numerical simulation to show that the surface signature of such eddies can decrease considerably while they (Added: are)still propagat(Replaced: ~~e~~ replaced with: ing) in the ocean interior.

The AREN that we can still track in the Southwest Atlantic, follow a quasi-zonal path, about 5° wide along the 35°S parallel which (Replaced: ~~broadens~~ replaced with: widens) further when passing (Deleted: ~~over~~)the Mid-Atlantic(Added: Ridge). They eventually reach the South American continental slope where (Replaced: ~~they~~ replaced with: the majority of them) propagate(Added: s) southward with the South Brazil Current. Here, they often merge with other anticyclones flowing south (Deleted: ~~ward~~) with the current and originating north of 20°S. Some AREN (Added: eddies)can be detected along the western slope of the South Atlantic as far south as the Zapiola gyre.

Our results suggest that Agulhas Rings can live longer than expected. The longest main (i.e., 0-order AREN) trajectory is more than 4 years old whereas, if we compute the travel time of the network (Replaced: ~~across~~ replaced with: through) lines C to G, we find a median time of 5 years for the trajectories connecting the eddies of the Southeast Indian Ocean to their (Replaced: ~~most distant~~ replaced with: furthest) destination in the Southwest Atlantic.

Our study reveals a different view of (Added: the)Agulhas Rings (Replaced: ~~than~~ replaced with: from) that provided in previous studies. However, it does not necessarily disagree with their (Replaced: ~~findings~~ replaced with: conclusions). Indeed, TOEddies is able to reconstruct a longer and more complete history of these eddies that encompasses the various Agulhas Rings segments of trajectories discussed in the literature.

The most important outcome of our study is probably the assessment of numerous eddy splitting and merging events (Replaced: ~~that involve~~ replaced with: involving) Agulhas Rings but also anticyclonic eddies of different origins(Added: ,) which leads to the formulation of the AREN. This (Deleted: ~~point~~)is essential (Replaced: ~~to better understand the dynamics of the ocean.~~ replaced with: for a better understanding of ocean dynamics.) Indeed, eddy separations and coalescences must induce a vigorous mixing of water masses advected in the core of the eddies, which has an important impact on the overall redistribution of the physical and biogeochemical water properties. As suggested by *Wang et al.* [2015], Agulhas Rings cannot be considered as coherent and isolated structures advecting the same water masses along their path. Therefore, our results provide a different (Replaced: ~~view~~ replaced with: perspective) on eddies (Replaced: ~~than~~ replaced with: from) most of the published studies that do not (Replaced: ~~take into account~~ replaced with: account for) eddy separations and merging events [e.g. *Chelton et al.*, 2011; *Haller and Beron-Vera*, 2013; *Faghmous et al.*, 2015; *Duacs/AVISO+*, 2017]. However, (Replaced: ~~while~~ replaced with: if) TOEddies can (Replaced: ~~infer~~ replaced with: deduce) the surface signature of eddies, (Deleted: ~~but~~)it is still limited (Replaced: ~~as~~ replaced with: because) it cannot access the exact processes involved in the evolution of eddies nor their subsurface structure.

Agulhas leakage plays an important role in the climate system, as a mechanism for transporting heat and salt between basins and closing the large scale overturning circulation [*Gordon*, 1985; *Beal et al.*, 2011]. In the context of global warming and (Replaced: ~~the first~~ replaced with: early) evidences of a changing Agulhas Current system and leakage [*Biastoch et al.*, 2008a; *Rouault et al.*, 2009; *Beal and Elipot*, 2016] our results highlight the role of Agulhas Rings as an important(Added: ,) albeit complex(Added: ,) vector for Indo-Atlantic exchange. They reveal a new long route for these eddies, (Replaced: ~~connecting unequivocally~~ replaced with: unequivocally connecting) the western boundary currents of the Indian and South Atlantic oceans.

However, although modeling studies using Lagrangian techniques suggest a direct connection between the Agulhas Leakage and the AMOC [*van Sebille et al.*, 2011; *Rühs et al.*, 2013] with more than 50% of the Agulhas Leakage reaching the North Atlantic, our study does not show a (Added: such)direct (Replaced: ~~connection of~~ replaced with: link for) the Agulhas Rings (Replaced: ~~with a northward flowing western boundary current in the South Atlantic north of 20°S~~ replaced with: a)s most of them recirculate southward with the South Brazil Current. (Replaced: ~~However~~ replaced with: Yet), a small number of these eddies (Replaced: ~~seem~~ replaced with: appear) to veer northward, crossing the Cruze(Added: i)ro do Sul and the Vitoria-Trinidade seamounts chains. These results leave open the question of how the connection between the Agulhas leakage and (Added: the)AMOC, as seen by the models, is achieved. Is the volume transport of these few eddies (Deleted: ~~flowing~~)north of 20° intense enough to close the AMOC transport budget? Are all these eddies the ones that make the connection or are most of them invisible from altimetry because they flow northward at depth, as subsurface eddies? Finally, do the Agulhas Rings really make the connection with the AMOC or is this achieved by circulating water around the mesoscale field?

(Replaced: ~~While~~ replaced with: Although) this study describes a(Replaced: ~~n~~ replaced with: much more complex) Agulhas leakage made by Agulhas Rings (Deleted: ~~much more complex~~)than previously observed, our results are still incomplete (Replaced: ~~as~~ replaced with: because) they cannot go beyond the limits of satellite altimetry. Indeed, altimetry maps are reconstructed from scattered observations that most probably affect the number of (Replaced: ~~eddies and trajectories that can be objectively recovered.~~ replaced with: objectively recoverable eddies and trajectories.) Moreover, these results are limited to the surface description of certain kinematic and dynamic properties. For a more in-depth description of these eddies and a quantitative estimate of the Agulhas leakage, future work should focus (Replaced: ~~on both, the three-dimensional varying~~ replaced with: both on the variable three-dimensional) structure of (Added: the)Agulhas Rings and (Deleted: ~~the~~)understanding (Deleted: ~~of~~)all the processes that govern the connection of the Agulhas Current system with the AMOC.

(Added: THE ENTIRE APPENDIX SECTION WAS ADDED FOR THIS REVIEW)

A: Validation of the TOEddies method and parameters

In this appendix, we describe in detail some aspects of the analyses and cross-validation presented in the core of the article.

A.1 Sensitivity of the algorithm on the persistence parameter

To assess the skill of the method, we developed a systematic procedure that tests the presence and properties of eddies against the "loopers", the independent eddy data set derived from surface drifting buoys by *Lumpkin* [2016] (LU16 in the following). This was used in the manuscript to infer the efficiency of the algorithm and to compare it to the database distributed by *Duacs/AVISO+* [2017] and based on *Chelton et al.* [2011] method and modified by *Schlax and Chelton* [2016].

This procedure was also used to test the sensitivity of TOEddies to its parameters and their value. These sensitivity studies have shown that the "persistence" is the most important parameter of the algorithm. This parameter, which prescribes a minimum value as an eddy amplitude threshold, is based on topological simplification studies [*Edelsbrunner et al.*, 2002; *Edelsbrunner and Harer*, 2010]. It is applied to isolate the local extremes of altimetric fields whose value is high enough to be considered robust in terms of signal-to-noise ratio. It can be compared to the minimum amplitude threshold often used in eddy detection algorithms found in the literature [e.g. *Chelton et al.*, 2011]. However, while the latter is applied to eddies after they have been identified, the persistence parameter is integral part of the eddy identification step of the TOEddies algorithm because it is used to select the altimetry extremes to be considered as eddies. This is to ensure, for example, the detection of the merging of two or more eddies, or the growth of a large eddy. Indeed, if the algorithm finds in a relatively large area more than one extreme, the TOEddies algorithm automatically identifies more than one eddy because it requires that the eddies should contain one and only one extreme. This is true unless all but one of the extremes have values below the threshold limit. In this case, TOEddies identifies a single large eddy and not two or more.

Four eddy data sets are presented in Table A.1 that lists the number of eddies identified by each of them and their detection efficiency expressed as a percentage of the total number of collocations with LU16 eddies. These datasets were created by varying the minimum amplitude threshold (i.e., the persistence) for the identified ADT extremes and are labelled accordingly: ADT_MinPersistenceThreshold. No tracking considerations were applied on them. Hence, ADT_01 corresponds to the ADT_raw data set presented in the core of the Article.

This parameter directly influences the number of eddies: when it is not zero, the higher is its value, the lower the number of detected eddies (Table A.1). We observed that this parameter has the greatest impact when it goes from a value of 0 mm to 1 mm, and less for values greater than 1 mm (see rows for ADT_00 and ADT_01 in Table A.1). In fact, a non-zero value, as small as 1 mm, for persistence increases the number of eddies detected. This is explained by the fact that it takes at least four grid points for an eddy to be defined as such by the method. When examining the effectiveness of matching TOEddies with LU16 loopers, a value of 1 mm compared to zero for the persistence parameter increases the matching by up to 8%. For threshold values greater than 1 mm there is no significant increase in the matching.

While a non-zero threshold value for persistence increases the number of detections, as well as the total area occupied by eddies and the efficiency of detecting eddies associated with LU16 loopers, it also increases the number of erroneous detections (computed as the mismatch in polarity between TOEddies and loopers) by a large fraction (up to 50%, see Table A.1). These errors increase with the threshold value. However, for a threshold value of 1 mm, they are negligible for eddies larger than 25 km (see Figure 8 in the main text). For these reasons, we chose the threshold value of 1 mm when applying TOEddies to altimetry maps.

A.2 Validation of the Eddy Detection Algorithms

The results of the cross-validation between LU16 and the different eddy satellite altimetry databases listed in Table 1 are discussed in detail below. Table 2 shows the number of eddies identified in each dataset and their detection efficiency expressed as percentages of the total number of collocations with LU16 eddies. To assess the skill of the method and provide quantitative comparisons between the different eddy datasets, a matching percentage is computed. It represents the proportion of each polarity of the LU16 eddies that were successfully cross-detected with eddies of the same polarity in

Table A.1. Eddy detection and collocation statistics with LU16 loopers for 4 data sets for the persistent threshold from 0 to 10 mm. The "max" annotation refers to the eddy contours associated with the maximum eddy azimuthal speed while the "out" annotation refers to the outer eddy contours. The percentages indicate the fractions of eddies by polarity as defined in LU16. Anti and Cyclo stand for respectively anticyclonic and cyclonic eddies.

Dataset	Number Eddies anti/cyclo [10^6]	Sum Area max anti/cyclo [10^{10} km^2]	Sum Area out anti/cyclo [10^{10} km^2]	Match Anti max / out [%]	Mismatch Anti max / out [%]	Match Cyclo max / out [%]	Mismatch Cyclo max / out [%]
ADT_00	3.1 / 3.2	2.7 / 2.4	4.1 / 3.8	63 / 66	1 / 2	69 / 71	1 / 1
ADT_01	3.2 / 3.3	3.2 / 2.8	5.2 / 4.6	66 / 71	2 / 3	71 / 75	1 / 2
ADT_05	3.1 / 3.2	3.1 / 2.8	5.2 / 4.6	66 / 71	2 / 3	71 / 75	1 / 2
ADT_10	2.8 / 2.9	3.1 / 2.7	5.2 / 4.6	66 / 71	2 / 3	70 / 75	1 / 2

each dataset (Table 2). Cross-detection errors are also defined as mismatches in eddy polarity or when several eddies detected by altimetry have been assigned to the same LU16 eddy.

The TOEddies detection algorithm was tested on the SLA and ADT maps (without applying an eddy lifetime threshold) to evaluate the most relevant altimetry dataset for automatic eddy detection. Table 2 shows that the TOEddies algorithm (referred to SLA_raw and ADT_raw) detects 34% (36%) more anticyclonic (cyclonic) eddies when SLA instead of ADT maps are used. The total area occupied by eddies derived from SLA is larger than that resulting from the use of the ADT field. This area is 31% (50%) higher than the surface encompassed by the eddy contour defined by R_{Vmax} for anticyclones (cyclones) and by 48% (65%) when the eddy boundary contour is defined by R_{out}.

When comparing the effectiveness of the results with LU16 and using the outer contour as eddy edge (Table 2), the ADT maps show a slightly better agreement for anticyclones (by about 2%) while the SLA maps give a slightly better result for cyclones (by about 3%). On the other hand, when the contour of maximum velocity is taken as the eddy boundary, the differences in detection efficiency between the SLA and ADT maps decrease in the case of cyclones while, for anticyclones, the ADT shows better results (4% more effective).

To validate the robustness of the TOEddies threshold requiring a minimum longevity of 4 weeks for a trajectory segment, the results of ADT_raw and TOEddies are compared. Table 2 shows that such a threshold reduces both the number and total extent of eddies. The number of eddies decreases by 25% and the total area they occupy by 10%. This is mainly due to the fact that the threshold over the eddy lifespan reduces the number of small eddies. In terms of validation compared to LU16, the number of collocations decreases for both cyclones and anticyclones when the time threshold is used (Table 2). This is particularly true for cyclones. Note here that the highest matching of the algorithm, independent of the time threshold or the altimetry field, is obtained for the eddy perimeters defined by the outer contour although there is a slight increase in errors.

As META2017 is probably the most widely used eddy atlas derived from satellite altimetry, in order to have another independent measure of the performance of our algorithm, we quantitatively compare META2017 and TOEddies overall statistics and skills. Table 2 suggests that META2017 identify 25% fewer eddies but their overall extent is

41% larger. Figure 7 shows the statistical distribution of META2017 and TOEddies radii. The distribution maximum is positioned at about 40 km for TOEddies and 60 km for META2017. A clear difference between cyclones and anticyclones appears in TOEddies where cyclones are, on average, smaller than anticyclones. This difference is also noticeable in META2017, but less marked. In TOEddies, fewer than 1% of the eddies have a radius greater than 140 km while it corresponds to 5% of the structures for META2017.

To compare the size of eddies detected by satellite altimetry with an independent variable related to mesoscale ocean dynamics, we estimated the first Rossby baroclinic radius (L_R). L_R characterizes regionally the size of long-lived eddies in the open ocean. The average value of L_R was calculated using the definition of *Chelton et al.* [1998] and the seven-year average (i.e. 2005 to 2012) of the World Ocean Database [*Boyer et al.*, 2013]. The resulting value is represented by the vertical dotted line in Figure 7. The shaded area represents L_R percentiles 10 and 90. This figure shows that TOEddies identifies structures whose size is comparable to L_R (around 60% of TOEddies radii are in the percentile range L_R 10 - 90) whereas this is not the case for META2017, for which less than 20% of radii are in this interval.

To ensure that the comparison of TOEddies and META2017 skill against LU16 loopers is as robust as possible in terms of measurement, TOEddies_rad statistics were used instead of TOEddies. Indeed, the TOEddies_rad and META2017 skills are obtained by considering equivalent eddy radii instead of eddy contours. Note here that the statistics for TOEddies and TOEddies_rad are very similar, only the skill decreases slightly. TOEddies_rad is 10% more efficient and its error in eddy detection is 3 times lower than META2017 in terms of eddy collocation with LU16. The ability of TOEddies_rad and META2017 to encompass LU16 eddy centers as a function of eddy size is shown in Figure 8. The percentage of matches with LU16 increases while the percentage of matching errors decreases for both atlases as the size of the LU16 vortex increases. Both datasets are more effective at detecting small cyclones than small anticyclones, and large anticyclones than large cyclones.

It can be expected that there will be a minimum size of eddies detected on satellite altimetry maps. The ability of the two atlases, TOEddies and META2017, to match LU16 eddies as function of LU16 size is presented in Figure 8. It shows that for a 25 km radius (which represents the average radius of the LU16 loopers, Figure 5 and the average grid size of the altimetry maps) more than 65% of the eddies are identified by TOEddies whereas they represent only 48% (52%) for the anticyclones (cyclones) in META2017. The 90% limit is reached for TOEddies for eddies with radii between 45 and 55 km, while it is 85-95 km (75-85 km) for anticyclones (cyclones) in META2017. In terms of detection errors (mismatching), they are less than 1% for anticyclones (cyclones) over 15 km (10 km) in the case of TOEddies, whereas for META2017, they become as small only for anticyclones (cyclones) larger than 30 km (70 km).

A.3 Validation of tracking filtering

In this section, we examine the ability of the two atlases, TOEddies and META2017, to track eddies. This ability is measured by looking at the proportion of the eddy collocation of the two atlases with LU16 loopers that participate in a trajectory that lasts more than a week. The total number of LU16 trajectories used in the comparison is 431 for anticyclones and 414 for cyclones. The comparison is presented here for the three versions of our atlas where we vary either the type of contours defining the eddy area (the outer contour and the maximum velocity contour) or by applying the same method in the collocation with LU16 as used for META2017.

Eddy trajectory comparison statistics are presented in Table A.2. Here, skill is measured by the overall percentage of matching between the TOEddies or META2017 and LU16 trajectories. The percentage of trajectories tracked is computed as the percentage of LU16 eddy trajectories of each polarity associated, for at least one day, with TOEddies or META2017 eddy trajectories of the same polarity. The "trajectory network" column shows the percentage of LU16 trajectories erroneously matched by more than one eddy in META2017 or by a first order network in TOEddies. The columns "> 50%" and "> 90%" indicate the number of LU16 trajectories collocated with the eddies defined by the other atlases during, respectively, more than 50 and 90 % of lifetime of the LU16 eddies. The "mean tracking time" column gives the average percentage of collocation time between LU16 eddies and those of the other atlases, expressed in terms of LU16 lifetime. The error estimates correspond to the collocation of eddies of different polarities for at least one day.

The results show that the TOEddies skill improves when the outer eddy contour (R_{out}) instead of the maximum velocity contour (R_{Vmax}) is used to define the eddy perimeter. However, the associated mismatches are somewhat larger. Taking into account both definitions of eddy limits, between 60% and 70% of LU16 trajectories are tracked by TOEddies and between 50 and 60% of them are tracked for more than 50% of their lifetime. The reconstruction of a higher order network is necessary for fewer than 10% of the trajectories successfully tracked. This could be a consequence of the LU16 filtering we performed before the validation processes. In fact, the merging and splitting of the eddies can cause sudden changes in the spin of the drifter and an increase in the radius of the LU16 loopers, a radius that can become greater than 300 km, the maximum limit we have set for them.

Using the radius for cross detection of structures gives results similar to those obtained using defined eddy perimeters. Table A.2 shows that the greatest difference in skill is obtained for META2017. Indeed, META2017 identifies between 5 and 10 % fewer trajectories than TOEddiesAtlas. Moreover, the percentages obtained for TOEddies indicate that trajectories that account for eddy merging and splitting are real and well reconstructed. On the other hand, the association of more than one META2017 trajectory with a LU16 trajectory suggests that META2017 sometimes loses the true eddy track. This is clear when considering the collocation time with LU16 loopers. Indeed, while between 1/2 and 1/3 of the TOEddies network recovers almost all LU16 trajectories (i.e. > 90 %), this statistic is only 1/4 for META2017. Moreover, META2017 trajectories follow LU16 loopers 10% less than TOEddies. META2017 mismatch cases are also more numerous (by a factor of two) than TOEddies cases.

Acknowledgments

The authors thanks the three anonymous reviewers for their constructive suggestions and relevant questions that improved the quality of the manuscript. The development of this work was made possible through the scientific visits of AC, CP and RL at IMARPE (Peru). RL had a financial support from the ‘Agence Nationale de la Recherche’ via the international mobility LabexMer, grant ANR-10-LABX-19-01 for this visit. The altimeter products were produced by Ssalto/Duacs and distributed by AVISO, with support from CNES. This work was supported by the European Union’s Horizon 2020 research and innovation programme under grant agreement no. 633211 (AtlantOS), a CNES-TOSCA research grant for SS and RL and the 11- ANR-56-004 grant for SS and BB; by the CNRS and INSU for BB ; IRD for AC and ANR DynEd Atlas for AC, CP and AS.

Table A.2. Tracking skill statistics for 4 collocated data sets with LU16 eddy trajectories that lasted at least 1 week. The percentage of trajectories tracked indicates the number of LU16 trajectories that are only associated with trajectories of the same polarity. The percentage of the trajectory network explains the percentage of trajectories poorly tracked in META2017 and properly tracked through the reconstruction of the first order network in TOEddies. The columns "> 50%" and "> 90%" indicate the number of LU16 trajectories collocated with the eddies defined by the other atlases during, respectively, more than 50 and 90 % of the life of LU16 eddies. The "mean tracking time" column gives the average percentage of collocation time between the LU16 loopers and the eddies of the other atlases expressed in terms of LU16 eddy life. The trajectory errors column indicates the number of trajectories associated, for at least one day, with an unmatched polarity eddy.

Dataset	limits	Trajectories tracked anti/cyclo [%]	% of trajectory network anti/cyclo [%]	Followed > 50% anti/cyclo [%]	Followed > 90% anti/cyclo [%]	Mean % time tracked anti/cyclo [%]	Trajectories errors anti/cyclo [%]
TOEAtlas	out	67 / 68	7 / 4	58 / 60	44 / 49	84 / 88	8 / 6
TOEAtlas	max	61 / 65	4 / 1	52 / 57	37 / 43	81 / 85	5 / 3
TOEAtlas_rad	max	58 / 63	6 / 4	49 / 54	34 / 40	81 / 84	4 / 5
META2017	max	48 / 58	3 / 7	35 / 41	26 / 27	73 / 70	9 / 8

References

Arhan, M., H. Mercier, and J. R. E. Lutjeharms (1999), The disparate evolution of three Agulhas rings in the South Atlantic Ocean, *Journal of Geophysical Research: Oceans*, *104*(C9), 20,987–21,005, doi:10.1029/1998JC900047.

Arhan, M., S. Speich, C. Messager, G. Dencausse, R. Fine, and M. Boye (2011), Anticyclonic and cyclonic eddies of subtropical origin in the subantarctic zone south of Africa, *Journal of Geophysical Research: Oceans (1978–2012)*, *116*(C11).

Ashkezari, M. D., C. N. Hill, C. N. Follett, G. Forget, and M. J. Follows (2016), Oceanic eddy detection and lifetime forecast using machine learning methods, *Geophysical Research Letters*, *43*(23), 12,234–12,241, doi:10.1002/2016GL071269, 2016GL071269.

Baker-Yeboah, S., D. A. Byrne, and D. R. Watts (2010), Observations of mesoscale eddies in the South Atlantic Cape Basin: Baroclinic and deep barotropic eddy variability, *Journal of Geophysical Research: Oceans*, *115*(C12), doi:10.1029/2010JC006236, c12069.

Ballegooyen, R. C., M. L. Gründlingh, and J. R. Lutjeharms (1994), Eddy fluxes of heat and salt from the southwest Indian Ocean into the southeast Atlantic Ocean: A case study, *Journal of Geophysical Research: Oceans*, *99*(C7), 14,053–14,070.

Beal, L. M., and S. Elipot (2016), Broadening not strengthening of the Agulhas Current since the early 1990s, *Nature*, *540*(7634), 570–573.

Beal, L. M., W. P. M. D. Ruijter, A. Biastoch, R. Zahn, M. Cronin, J. Hermes, J. Lutjeharms, G. Quartly, T. Tozuka, S. Baker-Yeboah, T. Bornman, P. Cipollini, H. Dijkstra, I. Hall, W. Park, F. Peeters, P. Penven, H. Ridderinkhof, and J. Zinke (2011), On the role of the Agulhas system in ocean circulation and climate, *Nature*, *472*(7344), 429–436, doi:doi:10.1038/nature09983, authors No 5 to 19 are members of the Working Group.

Biastoch, A., and C. W. Böning (2013), Anthropogenic impact on Agulhas leakage, *Geophysical Research Letters*, *40*(6), 1138–1143.

Biastoch, A., C. W. Böning, and J. R. E. Lutjeharms (2008a), Agulhas leakage dynamics affects decadal variability in Atlantic overturning circulation, *Nature*, *456*, 489–492, doi: doi:10.1038/nature07426.

Biastoch, A., J. R. E. Lutjeharms, C. W. Böning, and M. Scheinert (2008b), Mesoscale perturbations control inter-ocean exchange south of Africa, *Geophysical Research Letters*, *35*(20), doi:10.1029/2008GL035132, l20602.

Boebel, O., T. Rossby, J. Lutjeharms, W. Zenk, and C. Barron (2003a), Path and variability of the agulhas return current, *Deep Sea Research Part II: Topical Studies in Oceanography*, *50*(1), 35–56.

Boebel, O., J. Lutjeharms, C. Schmid, W. Zenk, T. Rossby, and C. Barron (2003b), The Cape Cauldron: a regime of turbulent inter-ocean exchange, *Deep Sea Research Part II: Topical Studies in Oceanography*, *50*(1), 57–86.

Boyer, T. P., J. I. Antonov, O. K. Baranova, C. Coleman, H. E. Garcia, A. Grodsky, D. R. Johnson, R. A. Locarnini, A. V. Mishonov, T. D. O'Brien, et al. (2013), World ocean database 2013.

Byrne, D. A., A. L. Gordon, and W. F. Haxby (1995), Agulhas Eddies: A Synoptic View Using Geosat ERM Data, *Journal of Physical Oceanography*, *25*(5), 902–917, doi: 10.1175/1520-0485(1995)025<0902:AEASVU>2.0.CO;2.

Capet, A., E. Mason, V. Rossi, C. Troupin, Y. Faugère, I. Pujol, and A. Pascual (2014), Implications of refined altimetry on estimates of mesoscale activity and eddy-driven offshore transport in the Eastern Boundary Upwelling Systems, *Geophysical Research Letters*, *41*(21), 7602–7610.

Carton, X. (2001), Hydrodynamical Modeling Of Oceanic Vortices, *Surveys in Geophysics*, *22*(3), 179–263, doi:10.1023/A:1013779219578.

Casanova-Masjoan, M., J. Pelegrí, P. Sangrà, A. Martínez, D. Grisolía-Santos, M. D. Pérez-Hernández, and A. Hernández-Guerra (2017), Characteristics and evolution of an Agulhas ring, *Journal of Geophysical Research: Oceans*, *122*(9), 7049–7065.

Chaigneau, A., and O. Pizarro (2005), Eddy characteristics in the eastern south pacific, *Journal of Geophysical Research: Oceans*, *110*(C6).

Chaigneau, A., A. Gizolme, and C. Grados (2008), Mesoscale eddies off Peru in altimeter records: Identification algorithms and eddy spatio-temporal patterns, *Progress in Oceanography*, *79*(2), 106–119.

Chaigneau, A., G. Eldin, and B. Dewitte (2009), Eddy activity in the four major upwelling systems from satellite altimetry (1992–2007), *Progress in Oceanography*, *83*(1), 117–123.

Chaigneau, A., L. T. Marie, E. Gérard, G. Carmen, and P. Oscar (2011), Vertical structure of mesoscale eddies in the eastern South Pacific Ocean: A composite analysis from altimetry and Argo profiling floats, *Journal of Geophysical Research: Oceans*, *116*(C11), doi:10.1029/2011JC007134.

Chelton, D. B., R. A. deSzoeke, M. G. Schlax, K. El Naggar, and N. Siwertz (1998), Geographical Variability of the First Baroclinic Rossby Radius of Deformation, *Journal of Physical Oceanography*, *28*(3), 433–460, doi:10.1175/1520-0485(1998)028<0433:GVOTFB>2.0.CO;2.

Chelton, D. B., M. G. Schlax, R. M. Samelson, and R. A. de Szoeke (2007), Global observations of large oceanic eddies, *Geophysical Research Letters*, *34*(15), n/a–n/a, doi: 10.1029/2007GL030812, l15606.

Chelton, D. B., M. G. Schlax, and R. M. Samelson (2011), Global observations of nonlinear mesoscale eddies, *Progress in Oceanography*, *91*(2), 167–216, doi: http://dx.doi.org/10.1016/j.pocean.2011.01.002.

Cipollone, A., S. Masina, A. Storto, and D. Iovino (2017), Benchmarking the mesoscale variability in global ocean eddy-permitting numerical systems, *Ocean Dynamics*, *67*(10), 1313–1333.

Cresswell, G. R. (1982), The Coalescence of Two East Australian Current Warm-Core Eddies, *Science*, *215*(4529), 161–164.

Cushman-Roisin, B., B. Tang, and E. P. Chassignet (1990), Westward motion of mesoscale eddies, *Journal of Physical Oceanography*, *20*(5), 758–768.

Dencausse, G., M. Arhan, and S. Speich (2010a), Routes of Agulhas rings in the southeastern Cape Basin, *Deep Sea Research Part I: Oceanographic Research Papers*, *57*(11), 1406–1421.

Dencausse, G., M. Arhan, and S. Speich (2010b), Spatio-temporal characteristics of the Agulhas Current retroflection, *Deep Sea Research Part I: Oceanographic Research Papers*, *57*(11), 1392–1405.

Doglioli, A. M., B. Blanke, S. Speich, and G. Lapeyre (2007), Tracking coherent structures in a regional ocean model with wavelet analysis: Application to Cape Basin eddies, *Journal of Geophysical Research: Oceans*, *112*(C5), doi:10.1029/2006JC003952, c05043.

Donohue, K. A., E. Firing, and L. Beal (2000), Comparison of three velocity sections of the Agulhas Current and Agulhas Undercurrent, *Journal of Geophysical Research: Oceans*, *105*(C12), 28,585–28,593, doi:10.1029/1999JC000201.

Drijfhout, S. S. (2003), Why anticyclones can split, *Journal of Physical Oceanography*, *33*(8), 1579–1591.

Duacs/AVISO+ (2014), A new version of SSALTO/Duacs products available in April 2014. Version 1.1, CNES., *[Available at http://www.aviso.altimetry.fr/fileadmin/documents/data/duacs/Duacs2014.pdf.]*.

Duacs/AVISO+ (2015), SSALTO/DUACS user handbook:(M) SLA and (M) ADT near-real time and delayed time products, *CLS-DOS-NT-06-034*, *6*, 74.

Duacs/AVISO+ (2017), Mesoscale Eddy Trajectory Atlas Product Handbook , *SALP-MU-P-EA-23126-CLS*, p. 17.

Edelsbrunner, H., and J. Harer (2010), *Computational topology: an introduction*, American Mathematical Soc.

Edelsbrunner, H., D. Letscher, and A. Zomorodian (2002), Topological persistence and simplification, *Discrete Comput Geom*, *28*, 511–533.

Elipot, S., and L. M. Beal (2015), Characteristics, Energetics, and Origins of Agulhas Current Meanders and Their Limited Influence on Ring Shedding, *Journal of Physical Oceanography*, *45*(9), 2294–2314, doi:10.1175/JPO-D-14-0254.1.

Faghmous, J. H., I. Frenger, Y. Yao, R. Warmka, A. Lindell, and V. Kumar (2015), A daily global mesoscale ocean eddy dataset from satellite altimetry, *Scientific Data*, *2*, 150,028, doi:10.1038/sdata.2015.28.

Frenger, I., M. Münnich, N. Gruber, and R. Knutti (2015), Southern ocean eddy phenomenology, *Journal of Geophysical Research: Oceans*, *120*(11), 7413–7449.

Garreau, P., F. Dumas, S. Louazel, A. Stegner, and B. Le Vu (submitted), High resolution in situ observations and tracking of a dual core anticyclonic eddy in the algerian basin, *submitted to Journal of Geophysical Research-Oceans*.

Garzoli, S. L., P. L. Richardson, C. M. Duncombe Rae, D. M. Fratantoni, G. J. Goñi, and A. J. Roubicek (1999), Three Agulhas rings observed during the Benguela Current Experiment, *Journal of Geophysical Research: Oceans*, *104*(C9), 20,971–20,985, doi:10.1029/1999JC900060.

Goni, G., S. Garzoli, A. Roubicek, D. Olson, and O. Brown (1997), Agulhas ring dynamics from TOPEX/POSEIDON satellite altimeter data, *Journal of Marine Research*, *55*, 861–883, doi:10.1357/0022240973224175.

Gordon, A. L. (1985), Indian-Atlantic transfer of thermocline water at the Agulhas retroflection, *Science*, *227*, 1030–1034.

Gordon, A. L., and W. F. Haxby (1990), Agulhas eddies invade the South Atlantic: Evidence from Geosat altimeter and shipboard conductivity-temperature-depth survey, *Jour-*

nal of Geophysical Research: Oceans, *95*(C3), 3117–3125.

Gordon, A. L., R. Weiss, W. Smethie, and M. Warner (1992), Thermocline and intermediate water communication between the South Atlantic and Indian Oceans, *J. Geophys. Res*, *97*, 7223–7240.

Griffa, A., R. Lumpkin, and M. Veneziani (2008), Cyclonic and anticyclonic motion in the upper ocean, *Geophysical Research Letters*, *35*(1), n/a–n/a, doi:10.1029/2007GL032100, l01608.

Guerra, L. A. A., A. M. Paiva, and E. P. Chassignet (Submitted), On the translation of Agulhas rings to the western South Atlantic Ocean, *Deep Sea Research*.

Haller, G., and F. J. Beron-Vera (2013), Coherent lagrangian vortices: The black holes of turbulence, *Journal of Fluid Mechanics*, *731*.

Halo, I., B. Backeberg, P. Penven, I. Ansorge, C. Reason, and J. Ullgren (2014), Eddy properties in the Mozambique Channel: A comparison between observations and two numerical ocean circulation models, *Deep Sea Research Part II: Topical Studies in Oceanography*, *100*, 38–53.

Herbette, S., Y. Morel, and M. Arhan (2004), Subduction of a surface vortex under an outcropping front, *Journal of physical oceanography*, *34*(7), 1610–1627.

Hernandez, F., P.-Y. Le Traon, and R. Morrow (1995), Mapping mesoscale variability of the Azores Current using TOPEX/POSEIDON and ERS 1 altimetry, together with hydrographic and Lagrangian measurements, *Journal of Geophysical Research: Oceans*, *100*(C12), 24,995–25,006, doi:10.1029/95JC02333.

Ioannou, A., A. Stegner, B. Le Vu, I. Taupier-Letage, and S. Speich (2017), Dynamical Evolution of Intense Ierapetra Eddies on a 22 Year Long Period, *Journal of Geophysical Research: Oceans*, *122*(11), 9276–9298.

Isern-Fontanet, J., E. García-Ladona, and J. Font (2006), Vortices of the Mediterranean Sea: An altimetric perspective, *Journal of physical oceanography*, *36*(1), 87–103.

Isoda, Y. (1994), Warm eddy movements in the eastern Japan Sea, *Journal of Oceanography*, *50*(1), 1–15.

Le Vu, B., A. Stegner, and T. Arsouze (2018), Angular Momentum Eddy Detection and tracking Algorithm (AMEDA) and its application to coastal eddy formation, *Journal of Atmospheric and Oceanic Technology*, *35*(4), 739–762.

Lehahn, Y., F. d'Ovidio, M. Lévy, Y. Amitai, and E. Heifetz (2011), Long range transport of a quasi isolated chlorophyll patch by an Agulhas ring, *Geophysical Research Letters*, *38*(16).

Lumpkin, R. (2016), Global characteristics of coherent vortices from surface drifter trajectories, *Journal of Geophysical Research: Oceans*, *121*(2), 1306–1321.

Lumpkin, R., and M. Pazos (2007), Measuring surface currents with Surface Velocity Program drifters: the instrument, its data, and some recent results, *Lagrangian analysis and prediction of coastal and ocean dynamics*, pp. 39–67.

Lutjeharms, J., and A. Gordon (1987), Shedding of an Agulhas ring observed at sea, *Nature*, *325*(6100), 138–140.

Lutjeharms, J. R. E. (2006), *The Agulhas current*, 342 pp., Springer-Verlag.

Lutjeharms, J. R. E., and R. C. V. Ballegooyen (1988), The Retroflection of the Agulhas Current, *Journal of Physical Oceanography*, *18*(11), 1570–1583.

Mason, E., A. Pascual, and J. C. McWilliams (2014), A New Sea Surface Height–Based Code for Oceanic Mesoscale Eddy Tracking, *Journal of Atmospheric and Oceanic Technology*, *31*(5), 1181–1188, doi:10.1175/JTECH-D-14-00019.1.

Matsuoka, D., F. Araki, Y. Inoue, and H. Sasaki (2016), A New Approach to Ocean Eddy Detection, Tracking, and Event Visualization–Application to the Northwest Pacific Ocean, *Procedia Computer Science*, *80*, 1601–1611.

McDonagh, E. L., K. J. Heywood, and M. P. Meredith (1999), On the structure, paths, and fluxes associated with Agulhas rings, *Journal of Geophysical Research: Oceans*, *104*(C9), 21,007–21,020.

McWilliams, J. C. (1985), Submesoscale, coherent vortices in the ocean, *Reviews of Geophysics*, *23*(2), 165–182.

Melander, M., N. Zabusky, and J. McWilliams (1988), Symmetric vortex merger in two dimensions: causes and conditions, *Journal of Fluid Mechanics*, *195*, 303–340.

Mkhinini, N., A. L. S. Coimbra, A. Stegner, T. Arsouze, I. Taupier-Letage, and K. Béranger (2014), Long-lived mesoscale eddies in the eastern Mediterranean Sea: Analysis of 20 years of AVISO geostrophic velocities, *Journal of Geophysical Research: Oceans*, *119*(12), 8603–8626, doi:10.1002/2014JC010176.

Nencioli, F., C. Dong, T. Dickey, L. Washburn, and J. C. McWilliams (2010), A Vector Geometry–Based Eddy Detection Algorithm and Its Application to a High-Resolution Numerical Model Product and High-Frequency Radar Surface Velocities in the Southern California Bight, *Journal of Atmospheric and Oceanic Technology*, *27*(3), 564–579, doi: 10.1175/2009JTECHO725.1.

Okubo, A. (1970), Horizontal dispersion of floatable particles in the vicinity of velocity singularities such as convergences, in *Deep sea research and oceanographic abstracts*, vol. 17, pp. 445–454, Elsevier.

Olson, D. B., and R. H. Evans (1986), Rings of the Agulhas current, *Deep Sea Research Part A. Oceanographic Research Papers*, *33*(1), 27–42.

Paul, M., T. van de Flierdt, M. Rehkämper, R. Khondoker, D. Weiss, M. C. Lohan, and W. B. Homoky (2015), Tracing the Agulhas leakage with lead isotopes, *Geophysical Research Letters*, *42*(20), 8515–8521, doi:10.1002/2015GL065625, 2015GL065625.

Pegliasco, C., A. Chaigneau, and R. Morrow (2015), Main eddy vertical structures observed in the four major Eastern Boundary Upwelling Systems, *Journal of Geophysical Research: Oceans*, *120*(9), 6008–6033.

Penven, P., V. Echevin, J. Pasapera, F. Colas, and J. Tam (2005), Average circulation, seasonal cycle, and mesoscale dynamics of the peru current system: A modeling approach, *Journal of Geophysical Research: Oceans*, *110*(C10).

Penven, P., J. R. E. Lutjeharms, and P. Florenchie (2006), Madagascar: A pacemaker for the Agulhas Current system?, *Geophysical Research Letters*, *33*(17), doi: 10.1029/2006GL026854, l17609.

Pujol, M.-I., Y. Faugère, G. Taburet, S. Dupuy, C. Pelloquin, M. Ablain, and N. Picot (2016), DUACS DT2014: the new multi-mission altimeter data set reprocessed over 20 years., *Ocean Science*, *12*(5).

Qiu-Yang, L., L. Sun, and L. Sheng-Fu (2016), Gem: a dynamic tracking model for mesoscale eddies in the ocean, *Ocean Science*, *12*(6), 1249.

Rae, C. M. D. (1991), Agulhas retroflection rings in the South Atlantic Ocean: an overview, *South African Journal of Marine Science*, *11*(1), 327–344, doi: 10.2989/025776191784287574.

Rhines, P. B. (1975), Waves and turbulence on a beta-plane, *Journal of Fluid Mechanics*, *69*(3), 417–443.

Rio, M., S. Guinehut, and G. Larnicol (2011), New CNES-CLS09 global mean dynamic topography computed from the combination of GRACE data, altimetry, and in situ measurements, *Journal of Geophysical Research: Oceans*, *116*(C7).

Rio, M.-H., S. Mulet, and N. Picot (2014), Beyond GOCE for the ocean circulation estimate: Synergetic use of altimetry, gravimetry, and in situ data provides new insight into geostrophic and Ekman currents, *Geophysical Research Letters*, *41*(24), 8918–8925, doi:10.1002/2014GL061773, 2014GL061773.

Rouault, M., P. Penven, and B. Pohl (2009), Warming in the Agulhas Current system since the 1980's, *Geophysical Research Letters*, *36*(12), doi:10.1029/2009GL037987, l12602.

Rühs, S., J. V. Durgadoo, E. Behrens, and A. Biastoch (2013), Advective timescales and pathways of Agulhas leakage, *Geophysical Research Letters*, *40*(15), 3997–4000.

Ruijter, W. d., A. Biastoch, S. Drijfhout, J. Lutjeharms, R. Matano, T. Pichevin, P. v. Leeuwen, and W. Weijer (1999), IndianâĂŘAtlantic interocean exchange: Dynamics, estimation and impact, *Journal of Geophysical Research: Oceans (1978–2012)*, *104*(C9), 20,885–20,910.

Sangrà, P., J. L. Pelegrí, A. Hernández-Guerra, I. Arregui, J. M. Martín, A. Marrero-Díaz, A. Martínez, A. W. Ratsimandresy, and A. Rodríguez-Santana (2005), Life history of an anticyclonic eddy, *Journal of Geophysical Research: Oceans*, *110*(C3), doi:10.1029/2004JC002526, c03021.

Schlax, M. G., and D. B. Chelton (2016), The "Growing Method" of Eddy Identification and Tracking in Two and Three Dimensions.

Schouten, M. W., W. P. M. de Ruijter, P. J. van Leeuwen, and J. R. E. Lutjeharms (2000), Translation, decay and splitting of Agulhas rings in the southeastern Atlantic Ocean, *Journal of Geophysical Research: Oceans*, *105*(C9), 21,913–21,925, doi:10.1029/1999JC000046.

Schouten, M. W., W. P. M. de Ruijter, and P. J. van Leeuwen (2002), Upstream control of Agulhas Ring shedding, *Journal of Geophysical Research: Oceans*, *107*(C8), 23–1–23–11, doi:10.1029/2001JC000804.

Schultz Tokos, K. L., H.-H. Hinrichsen, and W. Zenk (1994), Merging and migration of two meddies, *Journal of physical oceanography*, *24*(10), 2129–2141.

Simmons, H. L., and D. Nof (2000), Islands as eddy splitters, *Journal of marine research*, *58*(6), 919–956.

Smith, W., and D. Sandwell (1997), Global Sea Floor Topography from Satellite Altimetry and Ship Depth Soundings, *Science*, *277*(5334), 1956–1962.

Souza, J. M. A. C., C. de Boyer Montégut, C. Cabanes, and P. Klein (2011a), Estimation of the Agulhas ring impacts on meridional heat fluxes and transport using ARGO floats and satellite data, *Geophysical Research Letters*, *38*(21), doi:10.1029/2011GL049359, l21602.

Souza, J. M. A. C. D., C. De Boyer Montegut, and P.-Y. Le Traon (2011b), Comparison between three implementations of automatic identification algorithms for the quantification and characterization of mesoscale eddies in the south atlantic ocean, *Ocean Science*, *7*(3), 317–334.

Stammer, D. (1997), Global characteristics of ocean variability estimated from regional TOPEX/POSEIDON altimeter measurements, *Journal of Physical Oceanography*, *27*(8), 1743–1769.

Tierny, J., G. Favelier, J. A. Levine, C. Gueunet, and M. Michaux (2018), The topology toolkit, *IEEE transactions on visualization and computer graphics*, *24*(1), 832–842.

van Sebille, E., and P. J. van Leeuwen (2007), Fast northward energy transfer in the Atlantic due to Agulhas rings, *Journal of physical oceanography*, *37*(9), 2305–2315.

van Sebille, E., P. J. Van Leeuwen, A. Biastoch, and W. P. de Ruijter (2010), On the fast decay of Agulhas rings, *Journal of Geophysical Research: Oceans*, *115*(C3).

van Sebille, E., L. M. Beal, and W. E. Johns (2011), Advective time scales of Agulhas leakage to the North Atlantic in surface drifter observations and the 3D OFES model, *Journal of Physical Oceanography*, *41*(5), 1026–1034.

Veneziani, M., A. Griffa, A. M. Reynolds, and A. J. Mariano (2004), Oceanic Turbulence and Stochastic Models from Subsurface Lagrangian Data for the Northwest Atlantic Ocean, *Journal of Physical Oceanography*, *34*, 1884–1906, doi:10.1175/1520-0485(2004)034<1884:OTASMF>2.0.CO;2.

Villar, E., G. K. Farrant, M. Follows, L. Garczarek, S. Speich, S. Audic, L. Bittner, B. Blanke, J. R. Brum, C. Brunet, et al. (2015), Environmental characteristics of agulhas rings affect interocean plankton transport, *Science*, *348*(6237), 1261,447.

Wang, Y., M. Olascoaga, and F. Beron-Vera (2015), Coherent water transport across the South Atlantic, *Geophysical Research Letters*, *42*(10), 4072–4079.

Wang, Y., F. Beron-Vera, and M. Olascoaga (2016), The life cycle of a coherent lagrangian agulhas ring, *Journal of Geophysical Research: Oceans*, *121*(6), 3944–3954.

Weijer, W., W. P. de Ruijter, H. A. Dijkstra, and P. J. Van Leeuwen (1999), Impact of interbasin exchange on the Atlantic overturning circulation, *Journal of Physical Oceanography*, *29*(9), 2266–2284.

Weijer, W., W. P. De Ruijter, and H. A. Dijkstra (2001), Stability of the Atlantic overturning circulation: Competition between Bering Strait freshwater flux and Agulhas heat and salt sources, *Journal of Physical Oceanography*, *31*(8), 2385–2402.

Weijer, W., W. P. De Ruijter, A. Sterl, and S. S. Drijfhout (2002), Response of the Atlantic overturning circulation to South Atlantic sources of buoyancy, *Global and Planetary Change*, *34*(3), 293–311.

Weiss, J. (1991), The dynamics of enstrophy transfer in two-dimensional hydrodynamics, *Physica D: Nonlinear Phenomena*, *48*(2-3), 273–294.

Williams, S., M. Petersen, P.-T. Bremer, M. Hecht, V. Pascucci, J. Ahrens, M. Hlawitschka, and B. Hamann (2011), Adaptive extraction and quantification of geophysical vortices, *IEEE transactions on visualization and computer graphics*, *17*(12), 2088–2095.

Wunsch, C. (1999), Where do ocean eddy heat fluxes matter?, *Journal of Geophysical Research: Oceans (1978–2012)*, *104*(C6), 13,235–13,249.

Yi, J., Y. Du, Z. He, and C. Zhou (2014), Enhancing the accuracy of automatic eddy detection and the capability of recognizing the multi-core structures from maps of sea level anomaly, *Ocean Science*, *10*(1), 39.

Zheng, S., Y. Du, J. Li, and X. Cheng (2015), Eddy characteristics in the South Indian Ocean as inferred from surface drifters, *Ocean Science*, *11*(3), 361–371, doi:10.5194/os-11-361-2015.